ABSTRACT

Title of Thesis: DISCERNING THE ROLES OF OCEAN ACIDIFICATION, EUTROPHICATION, AND RIVER ALKALINIZATION IN DRIVING LONG-TERM PH TRENDS IN THE CHESAPEAKE BAY

Yijun Guo, Master of Science, 2022

Thesis Directed By: Professor Ming Li, Horns Point Laboratory, University of Maryland Center for Environmental Science

Rising anthropogenic CO_2 in the atmosphere and oceanic uptake of CO_2 have led to a gradual decrease in seawater pH and ocean acidification, but pH changes in estuaries and coastal systems are more complicated due to a multitude of global and regional environmental drivers. Increasing global fertilizer use due to agricultural production has led to a doubling of riverine nutrient loading since the 1950s, leading to widespread eutrophication in estuarine and coastal waters. Excessive nutrient loading stimulates primary production in the surface euphotic layer, which consumes CO_2 and elevates pH, but unassimilated organic matter sinks and decomposes in bottom waters, producing CO_2 and reducing pH. In the meantime, human-accelerated chemical weathering, such as acid rain and mining, has resulted in rising alkalinity in many rivers and basification in estuarine and coastal waters. To discern how these environmental drivers influence long-term pH trends in coastal waters, a coupled hydrodynamic-biogeochemical-carbonate chemistry model was used to conduct hindcast simulations of the Chesapeake Bay between 1951 and 2010. The model reproduced the observed chlorophyll increase and hypoxia expansion due to the increased nutrient loading. In contrast, low pH bottom

waters and acidic volume shrank from 1950 to 1980. GAM analysis of long-term pH trends in different regions of Chesapeake Bay revealed increasing pH in the upper Bay driven by the river alkalinization, a peak pH in the mid-Bay in the 1980s coincident with the peak nutrient loading and decreasing pH in the lower Bay driven by ocean acidification. Four scenario runs were performed to assess the individual effects of rising pCO_2, river alkalinization, riverine nutrient loading, and climate change (warming and sea-level rise) on long-term pH changes in the Chesapeake Bay. The model results suggested that river alkalinization was more important than ocean acidification in driving the long-term pH changes in the estuary.

DISCERNING THE ROLES OF OCEAN ACIDIFICATION, EUTROPHICATION AND RIVER ALKALINIZATION IN DRIVING LONG-TERM PH TRENDS IN THE CHESAPEAKE BAY

By

Yijun Guo

Thesis submitted to the Faculty of the Graduate School of the
University of Maryland, College Park, in partial fulfillment
of the requirements for the degree of
Master of Science
2022

Advisory Committee:

Professor Ming Li, Chair

Professor Weijun Cai

Associate Professor Jeremy M. Testa

Acknowledgements

I am extremely grateful to my advisor, Prof. Ming Li for his invaluable advice, continuous support, and patience during my master's study. His immense knowledge and plentiful experience have encouraged me in all the time of my academic research and daily life. I would also like to thank my academic committee member Prof. Jeremy Testa from CBL and Prof. Weijun Cai from University of Delaware. This research would not have been possible without their direct help and support.

And I am grateful to Wenfei Ni who provided the nutrient and wind data for the hindcast model and Chunqi Shen, who taught me a lot about the RCA-CC model.

I also want to thank Renjan Li and Yuren Chen who gave me a lot of precious advice on my study and thesis research. They were the most enjoyable people to work with. And I want to send my special thanks to Sophia and Carol who lived with me since the covid pandemic. They offered me the strongest supports in both my life and research. And I also want to thank Pinky who gave me a lot of emotional support when I was in stress.

And I really appreciate all the support and I received from my family and all the HPL staffs. Finally, I would like to thank NOAA for the financial support that allowed me to conduct this thesis.

Table of Contents

List of Figures

List of Tables

Chapter 1: Introduction

Since the beginning of the industrial era in 1760, the atmospheric CO_2 concentration has increased from 280 parts per million (ppm) to 400 ppm in 2019 (Friedlingstein et al. 2020). The oceans play an important role of absorbing CO_2 and regulating the atmospheric CO_2 concentration. Each year, nearly one third of the carbon emissions are absorbed into the upper ocean (Sabine et al. 2004). Consequently, the increase of anthropogenic carbon dioxide in atmosphere has led to the gradual decrease of pH in the surface ocean water, which is known as ocean acidification or referred as 'the other CO_2 problem' (Doney et al. 2009). The mean surface ocean pH declined around 0.1 unit and the aragonite saturation horizon in the open ocean became shallower since the pre-industrial era, which could have negative impacts on wide range of marine organisms that build shells from calcium carbonate (Orr et al. 2005, Doney et al. 2009, Logan 2010). Ocean acidification in the open ocean is a predictable phenomenon which does not suffer from many uncertainties associated with climate change forecasts (Doney et al. 2009). According to the Intergovernmental Panel on Climate Change (IPCC) AR5 report, the decrease in surface ocean pH is projected to be in the range of 0.20 to 0.21 for RCP (Representative Concentration Pathway) 6.0, and 0.30 to 0.32 for RCP8.5 between 1986–2005 and 2081–2100.

Coastal and estuarine environments provide important resources to human beings and are highly influenced by human activities. Compared to open ocean, multiple factors can change the natural balance of carbonate chemistry and pH in coastal water system. Therefore, it is worth asking whether coastal and estuarine systems are experiencing similar trends of acidification as the oceans, and how the coastal pH responds to both global and local influences. To answer this

question, observations of pH and carbonate chemistry parameters were made around the world. Unlike the open ocean surface pH, which has relatively low pH variations with a decreasing rate at approximately 0.002 units per year and diel to seasonal fluctuation between 0.024 to 0.096 unit (Doney et al. 2009, Hofmann et al. 2011, Carstensen and Duarte 2019), coastal pH generally has diverse trends and high variability, with diel to seasonal fluctuation up to 0.5 unit due to community metabolism or seasonal upwelling (Borges and Gypens 2010, Provoost et al. 2010, Cai et al. 2011, Hofmann et al. 2011, Duarte et al. 2013, Carstensen and Duarte 2019) and a broad span of long-term trends from −0.023 to 0.023 per year in different coastal systems (Borges and Gypens 2010, Provoost et al. 2010, Waldbusser et al. 2011, Carstensen and Duarte 2019). Therefore, there are other processes controlling the pH in coastal waters and ocean acidification is only one of many factors influencing pH changes in coastal areas. Based on the previous studies on coastal acidification, there are four main factors influencing the coastal and estuarine pH variability: (1) ecological metabolism and other redox reactions in water column; (2) river discharge (with high concentration of nutrients and organic matter); (3) hydrological mixing between the freshwater and ocean water; (4) climate change (such as ocean acidification and global warming)

1.1 Different impacts on coastal and estuarine pH

Net primary production in coastal system is generally one order of magnitude higher than that of open ocean (Gattuso et al. 1998, Duarte et al. 2013), and community metabolism is a big contributor to pH variations in coastal water systems (Borges and Gypens 2010, Provoost et al. 2010, Wallace et al. 2014). The primary production in the water column would fixes aqueous CO_2 and increases pH, but the respiration of the organisms releases CO_2 and decreases pH (Soetaert et al. 2007, Borges and Gypens 2010). The imbalance between the community production and respiration can lead to large diel to seasonal fluctuations in coastal water pH. For example, in

productive coastal systems with seagrass, coral reef, salt marsh or mangroves, the diel pH fluctuation can be up to 1.0 unit but the ecosystem is still CO_2-neutral in general (Duarte et al. 2013). During spring, more nutrients and organic matter are flushed into the estuarine water with increasing river discharge. The riverine nutrients and warm temperature in spring can stimulate phytoplankton bloom and increase pH, but lead to pH decreases in summer when water column respiration exceeds primary production. For example, in the southern bight of the North Sea (Brussaard et al. 1996) and Pearl River estuary (Dai et al. 2008) surface pH was found to increase approximately 0.5 in spring due to phytoplankton growth.

The decoupling of the production and respiration due to stratification or eutrophication can cause large pH changes in the coastal water (Borges and Gypens 2010, Cai et al. 2011). Increasing nutrient inputs from riverine water due to human activities like increasing application of chemical fertilizers can stimulate the growth of algae, increase the water turbidity and eventually lead to eutrophication (Boesch et al. 2001, Kemp et al. 2005a). During eutrophication, dissolved oxygen becomes depleted in the bottom water and CO_2 is released when the organic matter from the blooms is respired by bacteria (Sunda and Cai 2012). In semi-closed and eutrophic estuaries where seasonal stratification enhances the summer hypoxia and organic matter degradation under euphotic layer, the estuarine water is more vulnerable to the eutrophication-induced acidification. For example, low pH ($pH<7.5$) or large decrease of pH ($\Delta pH>0.5$) concurrent with DO decline in subsurface to bottom water were detected in many coastal systems during summer and fall months in US coast (like Long Island sound (Wallace et al. 2014), Chesapeake Bay (Kemp et al. 2005a, Brodeur et al. 2019)) and European coast (like Lake Grevelingen (Hagens et al. 2015) and Baltic sea (Sunda and Cai 2012)). But in shallow and well-mixed estuaries, CO_2 produced in water is more easily to be exchanged with atmosphere, and O_2 in the surface layer is better mixed down to

the deep water, and therefore, less vulnerable to the eutrophication-induced acidification (Wallace et al. 2014). For example, in well-mixed Belgian coastal water (Borges and Gypens 2010) and Dutch coast water (Provoost et al. 2010) the increased primary production due to nutrient increasing and eutrophication can override and even counter the effect of ocean acidification.

Except for the metabolism induced pH change discussed above, alkalinized water exported from rivers can also alter coastal and estuarine pH. For example, a long-term simulation of ocean acidification in the Northern Gulf of Mexico showed the coastal acidification progression was counteracted by the enhanced alkalinity from the Mississippi-Atchafalaya River System (Gomez et al. 2021). Also, an increase of surface water alkalinity was observed throughout the Baltic Sea from 1995 to 2014 which was attributed to terrestrial weathering process and internal alkalinity sources (Müller et al. 2016).

Except for the pH drivers discussed above, seasonal upwelling on the US west coast (Feely et al. 2008, Hauri et al. 2013) and Australia east coast (Schulz et al. 2019) are observed to lower coastal pH by bringing cold DIC-enriched and low pH deep water to the surface water, making the coastal system particularly prone to the effects of ocean acidification (Hauri et al. 2013). Alternatively, the carbonate chemistry within fresh riverine water have been found to directly influence the estuarine pH. Salisbury et al. (2008) found the coastal ecosystem can be acidified by the introduction of acidic river water. Hu and Cai (2013) found that estuaries with low to moderate riverine weathering product inputs exhibit a maximum pH decrease in the mid-salinity region as a resultof anthropogenic CO_2 intrusion and named the region ‘estuarian minimum buffer zone’(MBZ). Besides the factors mentioned above, there are more processes that can directly or indirectly affect the pH value in coastal and estuarine systems. For example, extreme weather events like storms can alter the water carbonate condition months after the storm event by

increasing riverine nutrient inputs, and further change the phytoplankton production (Johnson et al. 2013, Paerl et al. 2018, Osburn et al. 2019). Cai et al. (2017) found a pH minimum could exist in mid-depth estuarine water during summer when acid water produced through H2S oxidation is mixed upward from the anoxic deep water in Chesapeake Bay. Wind-driven lateral upwelling in the semi-closed estuary can enhance the release of respired CO_2 from subsurface water to the surface and alter the air-sea CO_2 flux (Huang et al. 2019). Thawing coastal permafrost and increasing river runoff due to melting ice can bring more DIC enriched water to the shelf water and amplify the impact of ocean acidification (Semiletov et al. 2016).

1.2 Long term trend in coastal pH and its impact on coastal organisms

With complex interactions in estuarine ecological system, Duarte et al. (2013) raised the question: is ocean acidification solely an open-ocean syndrome? Or in other words, are coastal and estuarine systems experiencing similar trends of acidification as the oceans? Baumann and Smith (2018) synthesized the diel to interannual variability of surface pH in 16 diverse, shallow-water habitats along the US coasts from 2002 to 2016. They found the overall interannual pH trend in these systems are quite diverse, with little to no spatial consistency even within regions along the US Atlantic, Gulf of Mexico, and Pacific coasts. Both positive and negative trends were detected in eastern and western coast and were one order of magnitude larger than the interannual trend in open ocean acidification. DO, salinity and temperature were found to be the possible factors related to the interannual trend of surface pH by affecting community metabolism state in these systems. But the correlation coefficient between these factors and interannual surface pH change were smaller than pH change in shorter scales (daily to monthly). The correlations between Chla concentration and pH were mostly nonsignificant, which means eutrophication induced

acidification in the shallow-water ecosystems can be less severe than that of the deep and stratified system.

Carstensen and Duarte (2019) summarized the long-term coastal pH trends over a wider range, including 11 coastal systems and 83 station observations from US, European and east Asian coasts between 1950s and 2010s. Well-mixed to stratified water systems, and weakly to strongly buffered water systems were included in the study. According to the results, long-term pH changes in coastal systems showed a broad span of range from −0.023 to 0.023 yr−1, with 65% of the ecosystems showing no monotonic trends, and 45% of the ecosystems studied showing positive trends, in contrast of the negative trends expected from CO_2 emissions. Weakly buffered or the permanently stratified (even highly buffered) coastal water, like permanently stratified Mariager Fjord in the Danish Straits, tend to have larger seasonal variation (about 1 unit). But the long-term pH trend did not show great difference between weakly or strongly buffered coastal systems. The highly diverse long-term pH trends suggested by this research indicates the nearshore pH may respond stronger to local drivers than global atmosphere pCO_2 rising and therefore, local management strategies can be more effective for maintaining healthy pH and DO levels in coastal habitats. However, none of the research investigated the long-term pH trend below the surface water, where are important habitats for bottom-dwelling, shell-forming organisms and more susceptible to eutrophication induced acidification, due to the lack of observations.

Estuarine and coastal waters are valuable habitats for many organisms. The extreme carbonate chemistry events (e.g. low pH) in the coastal water are known to be detrimental to the coastal dwelling organisms, especially the shell forming organisms. For example, abrupt and persistent breeding failures of Pacific oysters in shellfish hatcheries of Washington State coast in 2005-2009 are found to be related to coastal acidification partially induced by seasonal upwelling

of CO_2-enriched water (Feely et al. 2012). Also, Bohai Sea, China experienced scallop-breeding failures in 2011 summer because of large pH decline (up to 0.29 units) in bottom water due to red tide (Zhai et al. 2012). Long term gradual increase of CO_2 baseline can also influence the organisms by increasing extreme pH events in some coastal systems. For example, on the West Coast in California, a gradual increase in seawater pCO_2 since the beginning of industrial era has increased the frequency and intensity of the aragonite undersaturation periods in the water (Harris et al. 2013). Therefore, understanding the long-term carbonate chemistry dynamic and acidification trend in estuarine and coastal waters is very important for coastal resources management like selecting the hatchery sites and protecting the organisms under future climate change.

1.3 Chesapeake Bay acidification

Chesapeake Bay is the largest estuary in the US and provides valuable habitats for abundant commercially important organisms like blue crabs and oysters. It is approximately 300 km long reaching from Susquehanna River flat in the north to Mid-Atlantic Bight in the south with average depth around 6.5m. Its central channel is relatively deep and narrow which is 20-30m deep and 1-4 km wide (Kemp et al. 2005a). The Susquehanna River is the largest single contributor in the non-tidal watersheds feeding Chesapeake Bay in terms of river flow, nutrients and suspended sediment (Zhang et al. 2015). Chesapeake Bay is a partially mixed estuary affected by strong seasonal changes of the Susquehanna River discharge. The seasonal stratification in the bay starts to build up when Susquehanna River discharge is highest in winter and spring and reaches a maximum stratification during the summer. The lower layer estuarine return flow driven by the fresh and salt water mixing contributes to a longer residence times (90 to 180 d) for freshwater and nutrients (Kemp et al. 2005a). The high riverine nutrient input, seasonal stratification and long

residence time together make the Chesapeake Bay a productive system prone to eutrophication and hypoxia (Kemp et al. 2005a). As discussed in previous paragraphs, the process of hypoxia is usually coupled to the process of acidification in coastal and estuarine waters through the spatial decoupling of surface-layer primary production and deep water respiration. Therefore, Chesapeake Bay can also be vulnerable to the acidification driven by local stressors that drive eutrophication and hypoxia (Shen et al, 2019). Shen et al. (2020) did a 30-year simulation (1986-2015) using a coupled hydrodynamic-biogeochemical model to investigate anthropogenic impacts on long term pH trends in Chesaepeake Bay. The model results showed an overal increasing trend in upper bay pH that can be related to increasing alkalinization in Susquehanna River and a significant pH decline in lower bay associated with ocean acidification and lowered net ecosystem production. However, no modeling study was conducted during 1950-1985 when the riverine nutrient loading doubled and the riverine alkalinity increased from ~500 to ~900 μmol/kg.

1.4 Motivations and thesis structure

Increasing emissions of anthropogenic carbon into the atmosphere can lower open ocean pH. But the long-term pH trends in Chesapeake Bay are more complicated due to both global and regional drivers. The riverine nutrient export from Susquehanna River increased since 1950s due to the increasing use of fertilizer and detergent from land (Zhang et al. 2015). The increasing nutrients stimulated the development of eutrophication, which would elevate pH in the surface euphotic layer with increasing primary production and lower pH in the bottom layer with organic matter decomposition. On the other hand, long-term observations of alkalinity and pH in Susquehanna River demonstrated robust basification signals (Raymond and Oh 2009, Kaushal et al. 2013, 2018). The alkalinized water exported from the rivers can buffer the acidification and increase the estuarine pH. Surface water temperature in the bay was also found to increase at the

rate of 0.05 to 0.10 °C $year^{-1}$ over the past 30 years (Ding and Elmore 2015), and the relative sea level rise in bay also accelerated in last century and reached 4-10 mm $year^{-1}$ in 2011 (Ezer and Corlett 2012). The warming temperature can alter the CO_2 gas exchange with the atmosphere and influence the metabolism process in bay. Sea-level rise can increase water column stratification and contribute to the decoupling of production and respiration in estuarine water. However, due to the limited observation and complicated interactions within the system discussed above, the long-term trend of Chesapeake Bay acidification back to 1950s are not well understood.

In this study, we conducted a 60-year (1951-2010) retrospective simulation using a 3-D coupled hydrodynamic-biogeochemical mode (ROMS-RCA-CC). Reconstructed long-term carbon chemistry timeseries based on available historical observations were used to drive the 60-year simulation. Through the numerical experiments, we explored two main questions: (1) How did the long-term pH trends in Chesapeake Bay respond to local and global drivers over the sixty years? (2) How did the different global and regional environmental drivers impact the acidification in Chesapeake Bay? In Chapter 2, we introduced the methods used to reconstruct the historical carbon chemistry boundaries and analyzed the 60-year hindcast results that showed the long-term evolution of carbonate chemistry and other parameters in the estuary. In Chapter 3, we conducted four scenario runs to discern the impact of local and global stressors on long-term pH trends and compared the scenario model results with the hindcast results in Chapter 2.

Chapter 2: Long-term hindcast of carbonate chemistry in the Chesapeake Bay using a coupled hydrodynamic-biogeochemical model

2.1 Introduction

Chesapeake Bay had a long history of eutrophication and hypoxia dating back to 1950s (Hagy et al. 2004, Kemp et al. 2005a). Previous research found that the declining water quality was closely related to the increasing nutrient loading from Susquehanna River, which is the largest fresh water source to the Bay. Total nitrate/phosphate inputs from Susquehanna River to Chesapeake Bay doubled from 1950 to 1990/1970 respectively, then they declined afterwards due to improved watershed land management (Sprague et al. 2000) (Figure 2.1). The associated development of eutrophication and hypoxia may also influence pH variability by regulating the metabolic processes. Long-term observations of the major freshwater sources to Chesapeake Bay revealed robust basification signals, particularly in the Susquehanna River (Kaushal et al. 2013, 2018) and it may increase pH and the buffer capacity of the Chesapeake Bay water. Besides these local pH drivers, global changes like ocean acidification and warming can also affect Chesapeake Bay pH in the long run. Therefore, pH trends in Chesapeake Bay are much more complicated when compared to the ocean acidification which is solely caused by the rising CO_2 emission.

Few papers have addressed the long-term changes in the carbonate chemistry in Chesapeake Bay until recent years. Waldbusser et al. (2011) analyzed surface pH observations in Chesaepeak Bay from 1985 to 2008, and found a generally increasing trend in the mesohaline region of the mainstem Bay during summer and a decreasing trend in polyhaline surface water in both spring and summer seasons. But the causes behind these trends were not clear. To overcome

the constraint of limited observations, modelling was used as an approach to explore and explain the temporal and spatial changes in Chesapeake Bay pH. Shen et al. (2020) did a 30-year simulation (1986-2015) using coupled hydrodynamic-biogeochemical model to investigate anthropogenic impacts on longterm pH in Chesaepeake Bay. They found an overal increasing trend in upper bay pH that could be related to increasing alkalinization in Susquehanna River and a significant pH decline in lower bay associated with ocean acidification and lowered net ecosystem production. St-Laurent et al. (2020) used linked land–estuarine–ocean modeling system to understand the relative impacts of climate change and regional watershed changes on the carbon balance of the bay between the early 1900s and the early 2000s. They found the bay has turned from weak CO_2 source in 1900s to a CO_2 sink in 2000s. Although river basification and warming mitigated the CO_2 ingassing, rising atmospheric CO_2 and eutrophication still increased the total carbon intake over the century.

Due to sparsity in pH measurements before the 1980s and the lack of sustained DIC and TA measurements in the Bay, retrospective data analysis is inadequate to explore pH changes back to the 1950s when eutrophication and hypoxia started to form in Chesapeke Bay. In this study, we overcame this limitation by reconstructing long-term carbon chemistry timeseries based on available historical observations and running a 60-year (1951-2010) retrospective simulation using a 3D coupled hydrodynamic-biogeochemical model.

2.2 Method

2.2.1 Statistical and analysis approaches

Water quality parameters such as pH and riverine nutrients have complicated trends consisting of non-linear seasonal and interannual fluctuations. To detect the long-term trends in

these parameters, we used Generalized Additive Model (GAM) (Hastie and Tibshirani 2017). GAM is a generalized linear model with a linear predictor containing a sum of smooth nonparametric functions of covariates. It is favored over the generalized linear regression model because it allows for flexible specification of response by defining the model in terms of smooth functions rather than the detailed parametric relationships on the covariates (Wood 2006, James et al. 2013).

The GAM used in this research is shown as below:

$$y_t \sim y_{t-1} + s(dnum) + s(doy) + s(disc) + ti(dyear, doy) + ti(dyear, sal) + ti(dyear, doy, disc) \quad (2.1)$$

where y_t represents the response variables including pH, TA, DIC and riverine nutrients, y_{t-1} represents the same variables at the preceding time step, *dnum* is the number of month relative to the reference time (e.g. 1 for Jan. 1951), *doy* is the number of month in a year (e.g. 1 for January), and *disc* is the monthly averaged river discharge representing the influence of river flow. For the functions in GAM, *s()* is a smooth function with thin plate regression splines. *s(dnum)* denotes the long-term residual, *s(doy)* denotes the seasonal cycle, and *s(disc)* denotes effects of river flows on the interannual variabtions. *ti()* is tensor product of two smooth functions and indicates the interaction between the two variates. The high-order term *ti(dyear, doy)* represents the seasonal cycle over time and *ti(dyear, doy, disc)* represents the changing of seasonal river flow over time. The objective of GAM is to minimize the generalized cross-validation (GCV) score and maximize the model R^2 and percentage of deviation explained.

The non-parametric Mann-Kendall trend test (M-K test) was applied to the time series to statistically assess whether there is a monotonic trend of a variable over time (Mann 1945, Kendall

1948, Gilbert 1987). A monotonic trend means that the variable consistently increases (decreases) through time, but the trend may or may not be linear. In M-K trend test, data points were assumed to be not serially correlated over time and did not have to be normally distributed. In this research, M-K test is applied to both the external forcing such as air temperature, solar radiation, off-shore water level, as well as the state variables such as TA, pH, DIC in Chesapeake Bay. TA, pH and DIC that exhibit large seasonal and interannual variations. Therefore, GAM model was used to remove the short term signals before applying M-K test to detect the longterm trends of these time series.

To calculate the linear trends of the time series, we used the non-parametric Theil-Sen estimator (also called Sen's slope estimator) (Theil 1950, Sen 1968, Wilcox 2001). This estimator is a method for robustly fitting a line to sample points in a plane by choosing the median of the slopes of all lines through pairs of points. The significance level α was set as 0.05 for tests.

TA and pH in the Susquehanna river were found to be increasing over the past few decades but with large interannual variations (Raymond and Oh 2009, Kaushal et al. 2013). To estimate the linear trends of the riverine TA and pH we conducted Monte Carlo trend analysis. Monte Carlo trend analysis is a computational algorithm that relys on repeated random sampling to obtain the Sen's slope estimator in a timeseries (Zhang et al. 2004). By using this method, we assumed that normally distributed errors existed in the Susquehanna TA and pH measurements. We first randomly sampled the normally distributed errors 1000 times (pH error standard deviation=0.1, TA error standard deviation=10). Then we computed the pH (TA) as the sum of measured pH (TA) and random errors, and got 1000 possible sets of pH (TA) values for each time it was messured. Finally we calculated the Sen's slope on each set of the values and computed the fraction of the 1000 timeseries that had a significant trend ($\alpha<0.05$).

2.2.2 Reconstruction of model boundary TA and DIC

Since the measurement of carbonate parameters was insufficient and discontinuous before the 1980s, the reconstruction of historical riverine and oceanic carbon boundaries was the first step to conducting the retrospective simulation.

River boundary TA and pH from 1986 to 2010 in the Susquehanna River were obained from Chesapeake Bay Program (CBP) station CB1.0 and the other seven tributaries were obtained at nearby USGS stations according to Shen et al. (2019b). The Susquehanna River is the river with the longest TA and pH observation record. Susquehanna monthly TA and pH observations at the river boundary before the 1980s were obtained from USGS site 01540500 at Danville, PA, according to Raymond and Oh (2009).

To ensure the consistency of the TA and pH observations between Danville and CB1.0 stations, we compared the slopes of the time series using Monte Carlo analysis (Figure 2.2 and Figure 2.3). TA from Danville and CB1.0 shows an increasing rate of 9.9 μmol/kg per year and 10.56 μmol/kg per year, respectively. The two slopes had a difference of 0.57 μmol/kg per year, which can accumulate to 34.2 μmol/kg of difference for 60 years. And the slope of reconstructed TA was 10.01 μmol/kg per year (Figure 2.4(a)). Since three slopes were close to each other and the difference between two stations took up around only 6% of the total TA change from 1951 to 2010, we assumed the TA from Danville and CB1.0 were consistent despite the different locations. This long-term increase trend observed in Susquehanna TA time series was consistant with previous studies on river basification, which is considered to be caused by the decreased acid mine drainage, intense mineral weathering and mining activies since the 1940s (Raymond and Oh 2009, Kaushal et al. 2013).

For Susquehanna pH observations, we used the same method to examine the data consistency between the two stations (Figure 2.3). Observations of pH from Danville experienced three main steps of change. (1) From 1951 to the early 1960s, pH remained stable around the annual mean level of 7.00. (2) From mid 1960s to early 1980s, pH gradually increased from 6.71 to 7.71 at a rate around 0.055 per year. This riverine pH increase in later twentieth centuary was observed in many other main rivers in the eastern and midwestern US where the most population is located (Raymond and Oh 2009, Kaushal et al. 2018). While in wet years such as mid 1960s and 1970, pH dropped down to 6 because the stored acidity in the form of sulfate salts dissolved into water during flooding (Raymond and Oh, 2009). (3) After 1980s, pH was stable again around 7.76 with a small changing rate of -0.0016 per year. CB1.0 observation started from 1985 and the observation remained at the level around 7.63 with a small decreasing rate of -0.0008 per year. In the reconstructed pH time series (Figure 2.4(b), pH also showed a small changing rate at 0.0004 per year from 1980 to 2010 including the overlap time period between Danville and CB1.0 observations. From 1951 to 2010, the reconstructed pH increased at a rate of 0.014 unit per year (Figure 2.4(d)).

Riverine DIC concentrations during 1951-2010 were not measured, so we calculated DIC through CO2SYS program based upon available TA, pH, temperature and salinity etc. (Lewis and Wallace 1998). The calculated DIC also showed an overal increasing trend at 8.43 μmol/kg per year (Figure 2.4(c)). DIC to TA ratio is an important indicator of water acidity, higher ratio indicates higher CO_2 in the DIC pool and the system is more acidified and less bufferred against CO_2 change (Egleston et al. 2010). DIC to TA ratio decreased over the sixty years (Figure 2.4(d)), in agreement with the reported increaes of pH and acid buffer capacity in Susquehanna river since the 1950s (Kaushal et al. 2018).

TA in other seven tributaries before 1985 were calculated from empirical relationships between riverine TA and river discharge developed by Shen et al. (2019). And their corresponding DIC before 1985 were calculated based on the averaged DIC/TA ratio in each tributary from 1985 to 2010 when DIC and TA observations were avaliable (Table 2.1).

TA at the offhore ocean boundary was calculated from an empirical linear relationship (TA = 47.69*Sal + 640.77, r^2 = 95%) fitted with cruise data from the East Coast Program (Brodeur et al. 2019). The corresponding salinity at the ocean boundary was a depth-averaged climatology salinity from WOA (2013 V2) database. Ocean boundary DIC was calculated using the available oceanic boundary TA, salinity, seawater fCO_2 and SST using CO2SYS (Figure 2.5(d)). SST at the oceanic boundary was decadally averaged surfarce temperature from WOA (2013 V2). Seawater fCO_2 from 1982 to 2010 at the ocean boundary was obtained from Xu et al. (2020), who reconstructed Mid-Atlantic-Bight (MAB) surface water fCO_2 data using Bayesian-neural-network approach with 1° × 1° resolution in space and a monthly resolution in time. Seawater fCO_2 before 1982 was converted from seawater pCO_2 using CO_2 coefficients from Weiss (1974), where for surface waters $fCO_2 \approx 0.996\ pCO_2$ (Figure 2.5 (a)). To obtain the seawater pCO_2 before 1982, it was assumed that seawater pCO_2 before 1982 equals to atmosphere pCO_2 before 1982 plus averaged air-sea pCO_2 difference in 1982-2010:

$$sw\_pCO_{2\,1950\text{-}1982} = atm\_pCO_{2\,1950\text{-}1982} + \Delta pCO_2\_sw\text{-}air_{\,1982\text{-}2010} \quad (2.2)$$

Ocean boundary atmospheric pCO_2 was calculated from atmosphere CO_2 (atmospheric dry air mole fraction of CO_2), seawater temperature, and salinity according to Xu and Cai (2020):

$$atm\_pCO_2 = CO_2 * (1 - p_w), \quad (2.3)$$

where pw stands for water vapor pressure at the equilibrium temperature and salinity (Weiss and Price, 1980):

$$p_w=\exp(24.4543 - 67.4509 \times (100/T) - 4.8489 \times \ln (T/100) - 0.000554\times S) \quad (2.4)$$

Atmospheric CO_2 data from 2000 to 2010 came from Carbon Tracker, version CT2017 (http://carbontracker.noaa.gov), which is a data assimilation system built by the National Oceanic and Atmospheric Administration's (NOAA) Earth System Research Laboratory. To extend the temporal coverage back to 1950, we first calculated the average monthly difference between CarbonTracker data and the Mauna Loa CO_2 data (https://www.esrl.noaa.gov/gmd/ccgg/trends/data.html) for each grid point using data in the overlap period (2000–2015). And we applied this difference, which ranges from−2.8 to 8.5 uatm, to early years (1950–1999) when the CarbonTracker data were not available. Then the full set of atmospheric CO_2 data at the ocean boundary were obtained for the 6-decades from 1951 to 2010.

2.2.3 Coupled physical-biogeochemical model (ROMS-RCA-CC)

In this study, a coupled physical-biogeochemical model (ROMS-RCA-CC) was used to conduct the sixty-year retrospective simulation from 1951 to 2010 with constructed historical carbon boundary. Regional Ocean Modeling System (ROMS) model provided the simulations of hydrodynamics in Chesapeake Bay, which has been described and validated against the observations in previous studies (Li et al. 2005, Zhong and Li 2006). North American Regional Reanalysis (NARR) dataset was utilized to provide the essential atmosphere variables for the ROMS model in the period of 1984-2010. Twentieth Century Reanalysis (20CR) project dataset from NOAA-CIRES-DOE (National Oceanic and Atmospheric Administration-Cooperative Institute for Research in Environmental Sciences-Department of Energy)

(https://www.esrl.noaa.gov/psd/data/20thC_Rean/) was used to provide atmospheric variables in 1951-1983 when NARR data was not avaliable in the study area and wind speed was bias-corrected and scaled by month to NARR as a reference according to Ni and Li (In prep).

The Row Column Aesop (RCA) model is the biogeochemical model that simulates two phytoplankton groups, particulate and dissolved organic carbon, nitrogen, phosphorus, dissolved inorganic nitrogen, phosphorus, silica, and O_2. It also includes a two-layer sediment diagenesis module which simulates the cycling of carbon, nitrogen, phosphorus, silica, sulfur, and O_2 (Brady et al. 2013, Testa et al. 2013). The carbonate chemistry (CC) module was later coupled to RCA by Shen et al. (2019) to simulated the cycling of dissolved inorganic carbon (DIC), total alkalinity(TA) and aragonite CaCO3 in Chesapeake Bay. Riverine nutrient inputs in Cheseapeke Bay from 1951 to 2010 were obtained from reconstructed data from Ni and Li (In prep). The ocean boundary nutrient concentrations were acquired from WOA (2013) decadal average and from Filippino et al. (2011).

2.2.4 Retrospective simulation set up from 1951 to 2010

The model simulation was implemented for the years 1951 to 2010. The ROMS model was initiated in year 1950 as spin-up, then run continuously in the following 60 years with output at hourly intervals. The model has 120×80 horizontal grids (~1-2 km resolution) and 20 layers in vertical sigma-coordinate (Figure 2.6 (b)). The RCA model was run on the same grid as ROMS model at computational time-step of 450 seconds and the output was saved at 4-hourly interval. Since most of the organic matter generated in Chesapeake Bay is consumed within annual cycle (Cowan and Boynton 1996), RCA model was initiated every year with the spatial-interpolated condition of pervious December from the CBP observation during 1985-2010. The averaged nutrients initial condition for of 1985-1989 was set as the initial condition for 1970-1984 when the

river nutrient and organic matter input was at high level; it was scaled by 0.5 for 1950-1969 when the river input was at relatively low level (Ni and Li, in prep).

Model output of bottom pH and acidic volume were calculated and compared with limited measurements at Chesapeake Bay Institute and Chesapeake Bay Program monitoring stations(Figure 2.6 (a)). The along-channel and cross-channel developments of acidification over each decade during 1951-2010 were investigated. The statistical GAM model was utilized to identify the spatial and temporal changes of the modeled pH.

2.3 Results

2.3.1 Model evaluation of bottom pH and dissolved oxygen

Bottom pH and DO were calculated from retrospective model outputs and compared with historical observations made along the center axis of the Chesapeake Bay. The Chesapeake Bay Program (CPB) dataset provides bi-weekly water quality data observations in the main stem and nearby tributaries from 1984 to present. From 1949 to 1982, water quality data was measured less than once a month by the Chesapeake Bay Institute (CBI) . To cover the entire time period from 1951 to 2010, we chose four stations from CBP and four stations from CBI. Each pair of the two stations is close to each other (Figure 2.6 (a)).

The comparison between the monthly averaged model results and observation data showed that the model was able to reproduce the seasonal and interannual changes in bottom DO (Figure 2.8) and pH (Figure 2.7) along the central Chesapeake Bay over the sixty years. The correlation coefficients between the modeled and observed DO in three subregions varied from 0.8 to 0.95 ($p<0.05$) and the Root-Mean-Square-Error (RMSE) was small compared to the bottom DO variations. The pH correlation coefficients varied from 0.6 to 0.73 ($p<0.05$) in the upper and mid

bay. In the lower bay, the correlation coefficient in pH was around 0.2 ($p<0.05$). But since the pH observations in the lower bay were highly scattered, this mismatch between the model simulation and observational data may have resulted from the scarce data in both time and space.

Both the pH and DO time series showed large seasonal variations, with the highest value in winter and the lowest value in summer. Due to lower temperatures and higher wind speeds, stronger air-sea gas exchange and water column vertical mixing led to higher DO and pH in winter. The larger river discharge in spring set up the stratified structure of the esturiane water in summer, and the phytoplankton bloom in spring provided more organic matter in summer, which enhanced the respiration in bottom waters and further lowered DO and pH. A decreasing trend in the DO time series was found over the sixty years, and the reduction was larger in the early 1980s. But the bottom pH did not show an obvious long-term trend like the bottom DO from 1951 to 2010.

We also calculated the acidic (pH<7.5), hypoxic (DO<2 mg L^{-1}) and anoxic (DO<0.2 mg L^{-1}) volumes over the Cheseapeake Bay main stem from 1951 to 2010. There were no long-term bay-wide pH observations to estimate the acidic volume. But hypoxic and anoxic volumes were compared with measurement-based interpolations in July from Hagy et al. (2004) (Figure 2.9 (a)(b)). The lack of observations in both time and space may cause some of the mismatches between the model simulation and observation. Both the hypoxic and anoxic volumes showed an increasing trend around the 1970s. Hypoxia in Chesapeake Bay is sensitive to riverine nutrient increases (Hagy et al. 2004), but the acidification is the result of combined influences from both local and global drivers. Therefore, the acidic volume decreased from 1950s to 1980s and stablized afterwards. It also featured large interannual variations.

The summer (June-August averaged) hypoxia expanded from the 1950s to the 1980s, and the total volume increased from 2.9 km^3 to 6.3 km^3 (Table 2.2). Then the hypoxia volume slightly

decreased by around 8% to 5.8 km^3 in the 2000s. The alternative metrics cumulative hypoxia days (CHD, km^3days) followed similar pattern as the summer average hypoxic volume. The summer hypoxia usually started to develop in June and terminates in August. From 1950s to 1980s, the onset of hypoxia shifted earlier to May meanwhile the termination was delayed until early September. After the 1980s, the onset of hypoxia shifted a bit earlier while termination remained stable. The overall duration of hypoxia was prolonged by around 2 months from 1950s to 1980 but then it was shortened by around 10 days in 2000s.

The total acidic volume change had the opposite trend as compared to the hypoxic volume. From the 1950s to the 1970s, it first decreased from 9.22 km^3 to 7.95 km^3 (Table 2.3). Then the summer acidic volume increased by 30% to 10.17 km^3 in the 2000s. The alternative metrics cumulative acidification days (CHD, km^3days) decreased by 30% to 1128 km^3days from the 1950s to the 1980s and then it increased to 1272 km^3 days in the 2000s. Summer acidification initiated in March and terminated around August. From the 1950s to the 1980s, the initiation delayed from mid-March to early April. Then it shifted slightly ealier to late March in the 2000s. The termination shifted from late September to early October from the 1950s to the 1970s and then it stayed stable around early September after the 1970s. The overall duration of acidification fluctuated over the six decades and shortened by around one month from the 1950s to the 2000s.

2.3.2 Spatial and temporal distribution of carbonate chemistry

In this section, carbonate chemistry related variables in Chesapeake Bay are described by decadal averages (1950-1959, 1960-1969, 1970–1979, 1980–1989, 1991–1990, and 2001-2010) to facilitate our analysis of the spatial distribution of these variables. Both spring and summer averages were calculated to explore the seasonal changes. Spring season includes March, April, and May while summer season includes June, July, and August.

The along-channel distributions of carbonte chemistry related variables in summer and spring were plotted to better understand the pH change described in previous sections (Figure 2.10 2.11). In general, the salinity distribution represents the physical mixing between fresh and oceanic water in the along-channel direction. Seawater with higher salinity intruded from the bottom of the estuary's mouth and the salt intrusion penetrated further landward from 1951 to 2010 due to the sealevel rise. TA is a relatively conservative variable because CO_2 from air-sea exchange or biological respiration does not directly influence its concentration in the water. So the overall distribution of TA was similar to the salinity distribution. The increase of TA in the esturine head agreed with the basification trend obeserved in the Susquehanna River (Raymond and Oh 2009). The distribution of DIC was also influenced by the fresh-salt water mixing with high DIC seawater in the lower layer. But the vertical gradient of DIC was larger than that of TA due to the phytoplankton production in surface water and the organic matter decomposition in deep water. From the 1950s to the 1980s, the DIC vertical gradient increased due to the increasing phytoplankton biomass as represented by chlorophyll-a (CHLA). Both TA and DIC had lower vertical gradients and lower concentration in spring.

Low pH water (pH<0.5) expanded seaward from the upper bay bottom water due to low DIC and TA concentration river flow combined with high rates of terrestrial organic matter respiration (Shen et al. 2019). And the low pH water volume stayed in the location between 37.7^{o}N and 39.5^{o}N over the sixty years. The minimum pH (pH as low as 7.0) existed during summer in the bottom water around 39^{o}N in the summer hypoxic zone of the main stem related to bottom organic matter respiration. Minimum pH volume fluctuated with time with the highest volume in 1970s and lowest volume in the 1980s. The pH in the lower bay was high (pH up to 8.0) and had

smaller vertical gradients because of the highly buffered seawater intrusion and strong mixing. But the overal lower bay pH decreased over the six decades due to the ocean acidification.

In general, surface DO was higher than bottom DO, and spring bottom DO was higher than summer bottom DO. In summer, the water colume with low DO (DO<2 mg/L) was around 39^{o}N to 38.5^{o}N. And the summer hypoxic water volume had an overall incresing trend with the increase of eutrophication from 1950s to 1980s. The largest hypoxic volume was in the 1980s when phytoplankton biomass reached its maximum in the sixty years.

2.3.3 Long-term pH trends in Chesapeake Bay

In this section, we further inspected the longterm trend of pH change in Chesapeake Bay over the sixty years. We first calculated the decadal average acidification timing and duration change. Then we analyzed the sub-regional average pH long term trend by using the GAM fit model and the M-K trend test.

The long-term residual in the GAM fit to the regionally averaged pH, namely *s(dnum)* in equation 2.1, is shown in Figure 2.12. The surface and bottom pH showed similar trends in different sections of the bay. In the upper bay, pH showed an overall increasing trend with some fluactuation over the last sixty years. From 1951 to 2010, surface pH increased by around 0.1. But bottom pH was more fluctuated with an increase from the 1950s to 1980s by around 0.1 then a slight decrease of 0.05 after 1980. Mid-bay pH first increased from the 1950s to the 1980s by 0.15, then slightly decreased by 0.08 after the 1980s. The peak pH in 1980s coincided with peak phytoplankton biomass when the nutrient loading was largest In the lower bay, surface pH increased by around 0.8 from 1951 to 1980, then decreased back to the 1950s level at the end of

the 2000s. Lower bay bottom pH showed a more obvious decreasing trend, and pH decreases by around 0.05 over sixty years.

We also calculated the spring and summer average pH in different sections of the bay to better understand the long-term trend of pH over the sixty years (Figures 2.13, 2.14). The result revealed an overall increasing trend in the upper bay and a decreasing trend in the lower bay. While in the mid bay, pH was relatively stable over the sixty years. The M-K trend test was applied to the seasonal time series to detect long-term trends (Table 2.4). Statistically significant declining rates were found in the lower bay pH in both spring and summer. And the decline rates in summer were generally larger than in spring. In summer, surface and bottom pH in the lower bay decreased at the rate of -0.017 and -0.033 units per decade, respectively. In spring, bottom pH decreased at a rate of -0.025 units per decade, while surface pH in the lower bay did not have a significant trend. In the upper bay, a basification signal was detected in both surface and bottom water during spring. Upper bay pH increased at a rate of 0.078 units per decade in surface water and 0.057 units per decade in bottom water. While in summer, the basification trend was not statistically significant. It suggests that the pH trend in the upper bay may be influenced by the river basification signal observed in nearby main tributaries (Kaushal et al. 2018) and this signal was strongest during the spring when the river flow was highest. Although no statistically significant linear trends were found in the mid-bay over the sixty years, we noticed the mid bay pH trend consisted of an increasing trend from the 1950s to 1980s and a decreasing trend after the 1980s. Other factors like phytoplankton biomass which peaked in 1980s may affect pH changes in the mid-bay.

2.4 Discussion and Conclusion

In this study, we investigated Chesapeake Bay acidification over a long-term period (1951–2010) using a coupled hydrodynamic-biogeochemical model. This long-term retrospective

simulation successfully captured the seasonal and interannual variations of bottom pH along the central bay from 1951 to 2010, and it also reproduced the larger phytoplankton biomass and hypoxia expansion with increasing nutrient loading between 1950s and1980s. The modeled temporal and spatial distribution of carbonate chemistry displayed the signals of basification, eutrophication, ocean acidification, and sea-level rise in different sections of the bay over the sixty years. These local and global drivers can together influence the long-term pH variation in Chesapeake Bay.

The model revealed an overall increasing pH trend in the upper bay and a decreasing pH trend in the lower bay, while the mid-bay pH was relatively more stable over the sixty years. Upper bay pH had a stronger basification signal in spring than in summer. And it increased at a rate of 0.057 to 0.078 units per decade during spring, which could be related to the river basification signal observed in nearby main tributaries (Kaushal et al. 2018). Lower bay bottom pH had bigger decreasing rate in summer than spring. In summer, the lower bay bottom pH decreased at a rate of -0.033 units per decade and surface water pH decreased at a rate of -0.017 units per decade. The lower bay surface pH decrease rate was close to the Mid-Atlantic-Bight surface pH decadal change (-0.016 ± 0.002 units per decade) from 1985 to 2015 (Xu et al. 2020). It may indicate that the lower bay pH decrease can be mostly attributed to ocean acidification from increasing atmospheric CO_2. The mid-bay pH showed large fluctuations over the sixty years, and it can be a reflection of the combined impact of local and global pH divers.

To better compare our modeled results with previous research, we calculated the seasonally averaged surface water pH trends from 1985 to 2010 (Figure 2.15). The modeled pH showed an overall increasing trend in the upper bay with 0.0063 unit per year in spring and 0.0024 unit per year in summer. A decreasing trend was found in both mid and lower bay. The mid-bay spring

surface pH showed an decrease of -0.0039 unit per year and summer surface pH showed an bigger decrease of -0.0049 unit per year. And the lower bay show pH showed an decreasing slope of -0.0043 unit per year in spring and -0.0040 unit per year in summer. These seasonal trends agree with the 30-year (1985-2015) hindcast pH trends from Shen et al. (2020). The latter results came from the same hydrodynamic-biogeochemical-carbonate chemistry model, grids and similar boundary forcing as this research. The difference between the two set of trends ranges from 0.0001 to 0.002 which indicates the consistency of the two experiments. This difference may contribute to the additional 5 years (2011-2015) from Shen et al. (2020) that is not covered in this research. Waldbusser et al. (2011) also did similar trend analysis on seasonal daytime surface pH based on the Chesapeake Bay Program observations from 1985 to 2008. Their results revealed an decline in polyhaline (lower part of the bay) surface water pH with a slope of 0.012 unit per year in spring and 0.006 unit per year in summer. While an increase in mesohaline water (upper and mid part of the bay) during summer was detected with a slope of 0.005 unit per year. The differences between our modeled seasonal pH trends and observational trends from Waldbusser et al. (2011) could be resulted from the mismatch in space and time. Waldbusser et al. (2011) focused the daytime pH trends but our study calculated the daily averaged pH value. And the pH in the Chesapeake Bay can vary in the range of 0.2 to 0.5 unit in a day (Shen et al. 2019). Also, we calculated the spatially avergaed pH based on our model grids in the main stem of the bay which is not the same as the observational stations used by Waldbusser et al. (2011) that are closed to the tributaires. Besides, our modeled pH were calculated from the CO2SYS program based on TA and DIC which can also leads to some error compared to the observations.

The spatial and temporal distributions of carbonate chemistry demonstrated the impact of eutrophication development on Chesapeake Bay pH. A significant increase of spring surface

chlorophyll-a concentration from 1950s to 1980s was detected (Figure 2.11). The increased spring phytoplankton bloom is a reflection of the development of eutrophication from 1950s to 1980s which is consistent with the increased riverine nutrient export from the Susquehanna River (Figure 2.1)(Kemp et al. 2005). At the same time summer hypxia expanded with the development of eutrophication (Figure2.10). Previous research found eutrophication can exacerbate acidificatiotion in mutiple esturiane and coastal systems including northern Gulf of Mexico and East China Sea (Feely et al. 2010, Cai et al. 2011, Wallace et al. 2014, Laurent et al. 2017). The unassimilated organic matter from the spring bloom sinks and decomposes in bottom waters during summer which further produce CO_2 and lower bottom pH. But our study shows the summer bottom pH increased from 1960s to 1970s. paralleling with the increase of riverine pH from 1960 to 1980. It may indicate that the significant river alkalinization signal from Susquehanna River during the 1960s and 1970s had a bigger influence on mid bay pH than eutrophication.

As for the acidic and hypoxic volumes, acidification in Chesapeake Bay did not show a clear expansion over the sixty year unlike the obvious hypoxia expansion from eutrophication. The total acidic volume first decreased from 9.22 km^3 to 7.95 km^3 by 16% from the 1950s to 1970s then increased by 30% to 10.17 km^3 in the 2000s. The overall duration of acidification fluctuated over the six decades and shortened by around one month from the1950s to 2000s with both later onset and earlier termination of about two weeks.

Since limited observation data were available before the 1980s, this study relied on numerical model simulation instead of observation data to reconstruct the development of acidification in Chesapeake Bay. Although a numerical model is never perfect at reproducing reality, with proper validation, it can still represent the general response of the system when the

external forcing changes with high-resolution data in both time and space. Thus, model simulation was less sensitive to the sampling bias than observation, as described in Section 2.3.1.

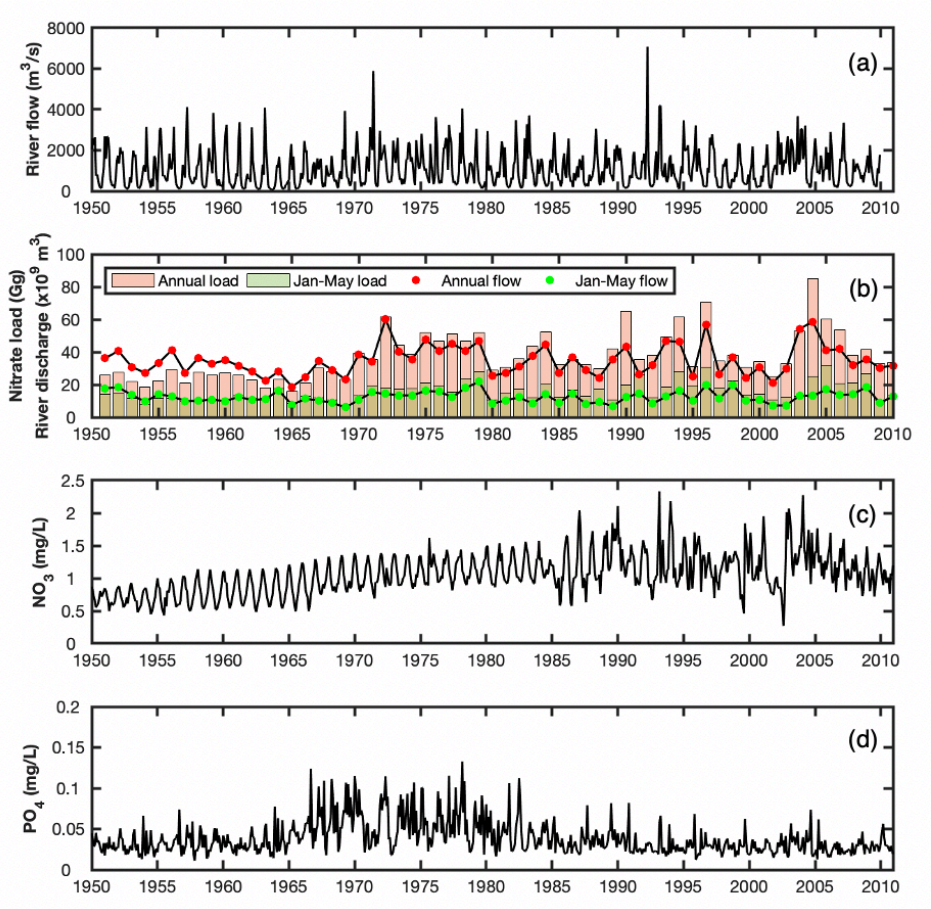

Figure 2.1 (a) Monthly freshwater discharge of Susquehanna River from 1950 to 2010. (b) Jan-May and annual average river discharge/nitrate load of Susquehanna River. (c) Estimated monthly average nitrate concentration of Susquehanna River from 1950 to 2010 from Zhang et al. (2013). (d) Monthly average phosphate concentration of Susquehanna River from 1950 to 2010.

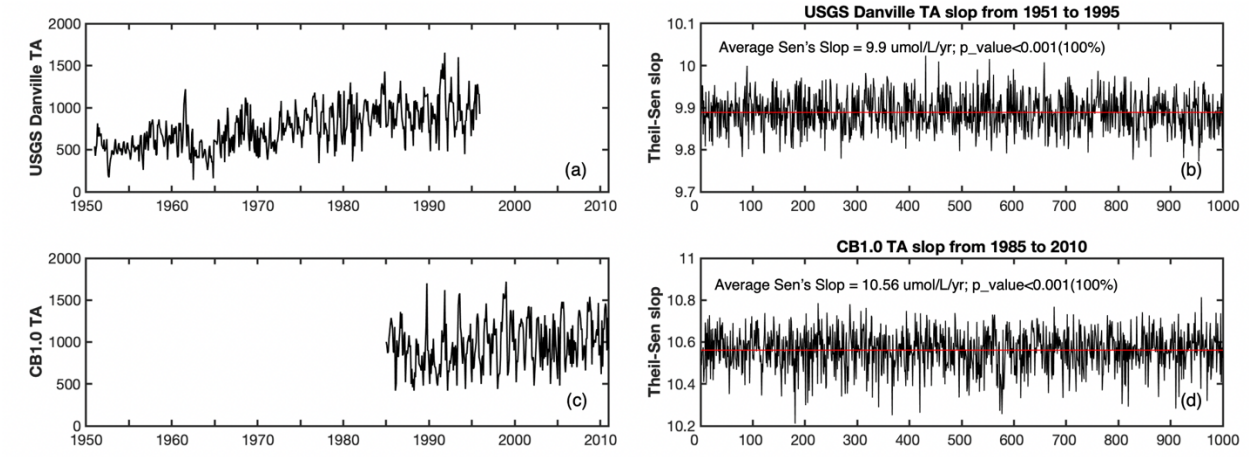

Figure 2.2 (a) Susquehanna River TA observation from USGS Danville station. (c) Susquehanna River TA observation from CBP CB1.0 station. (b) Monte Carlo trend analysis of USGS Danville TA. The average Sen's slope of the 1000 TA timeseries is 9.9 μmol/kg/year with 100% of the timeseries has a p value less than 0.001. (d) Monte Carlo trend analysis of CB1.0 TA. The average Sen's slope of the 1000 TA timeseries is 10.56 μmol/kg/year with 100% of the timeseries has a p value less than 0.001.

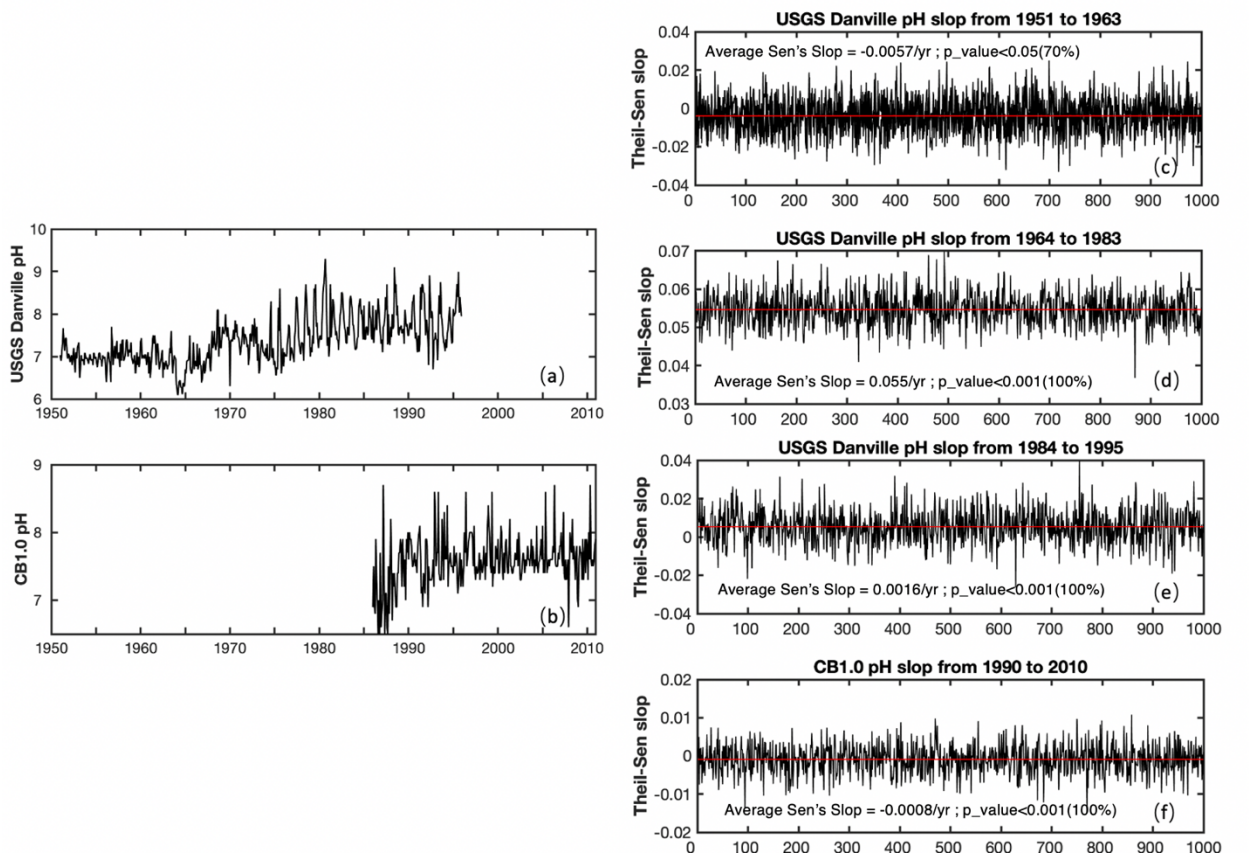

Figure 2.3 (a) Susquehanna River pH observation from USGS Danville station. (b) Susquehanna River pH observation from CBP CB1.0 station. (c) Monte Carlo trend analysis of USGS Danville pH from 1951 to 1963. The average Sen's slope of the 1000 pH timeseries during this period is -0.0057 unit/year with 70% of the timeseries has a p value less than 0.05. (d) Monte Carlo trend analysis of USGS Danville pH from 1964 to 1983. The average Sen's slope of the 1000 pH timeseries is 0.055 unit/year with 100% of the timeseries has a p value less than 0.001 (e) Monte Carlo trend analysis of USGS Danville pH from 1984 to 1995. The average Sen's slope of the 1000 pH timeseries is 0.0016 unit/year with 100% of the timeseries has a p value less than 0.001 (f) Monte Carlo trend analysis of CB1.0 pH from 1990 to 2010. The average Sen's slope of the 1000 pH timeseries is -0.0008 unit/year with 100% of the timeseries has a p value less than 0.001

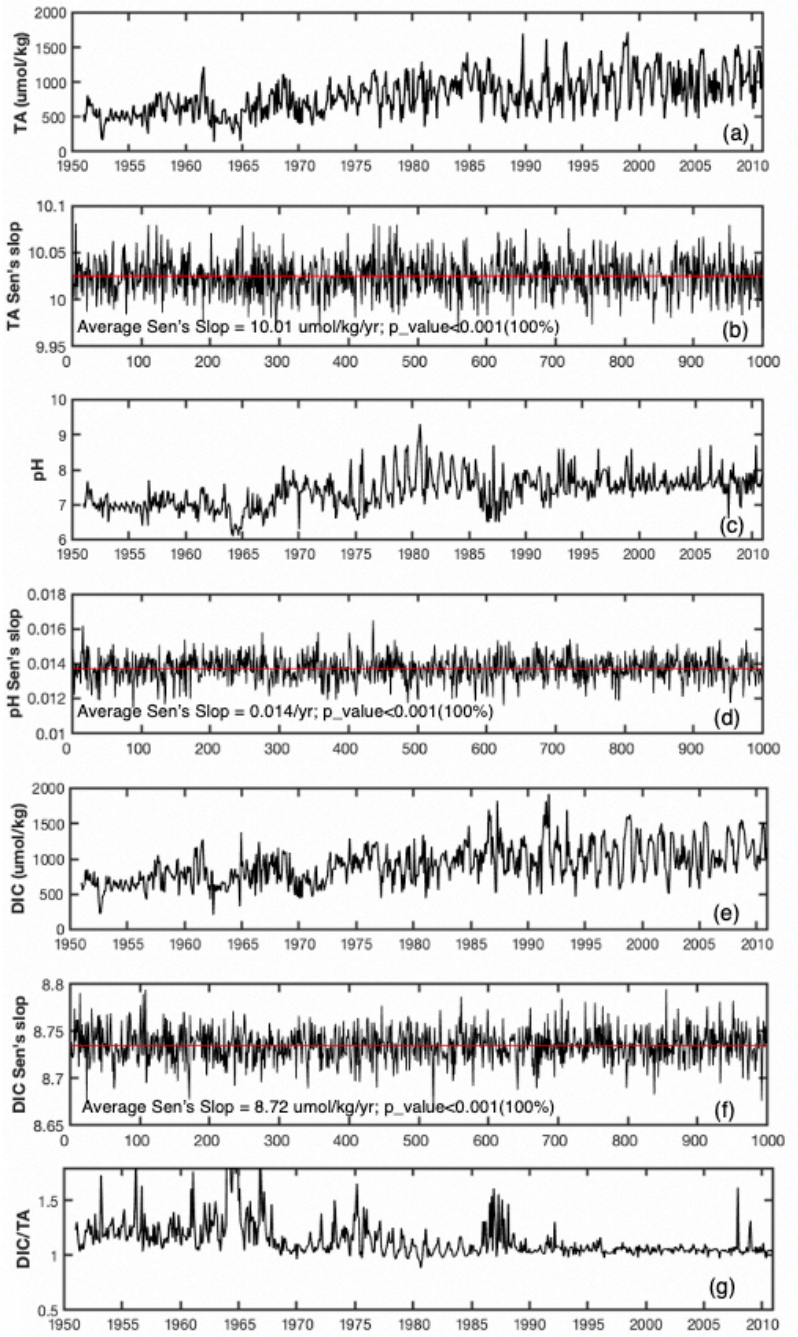

Figure 2.4 (a) Reconstructed Susquehanna TA from 1951 to 2010. (b) Reconstructed Susquehanna pH from 1950 to 2010. (c) Calculated Susquehanna DIC from 1951 to 2010. (d) Calculated DIC/TA ratio from 1951 to 2010.

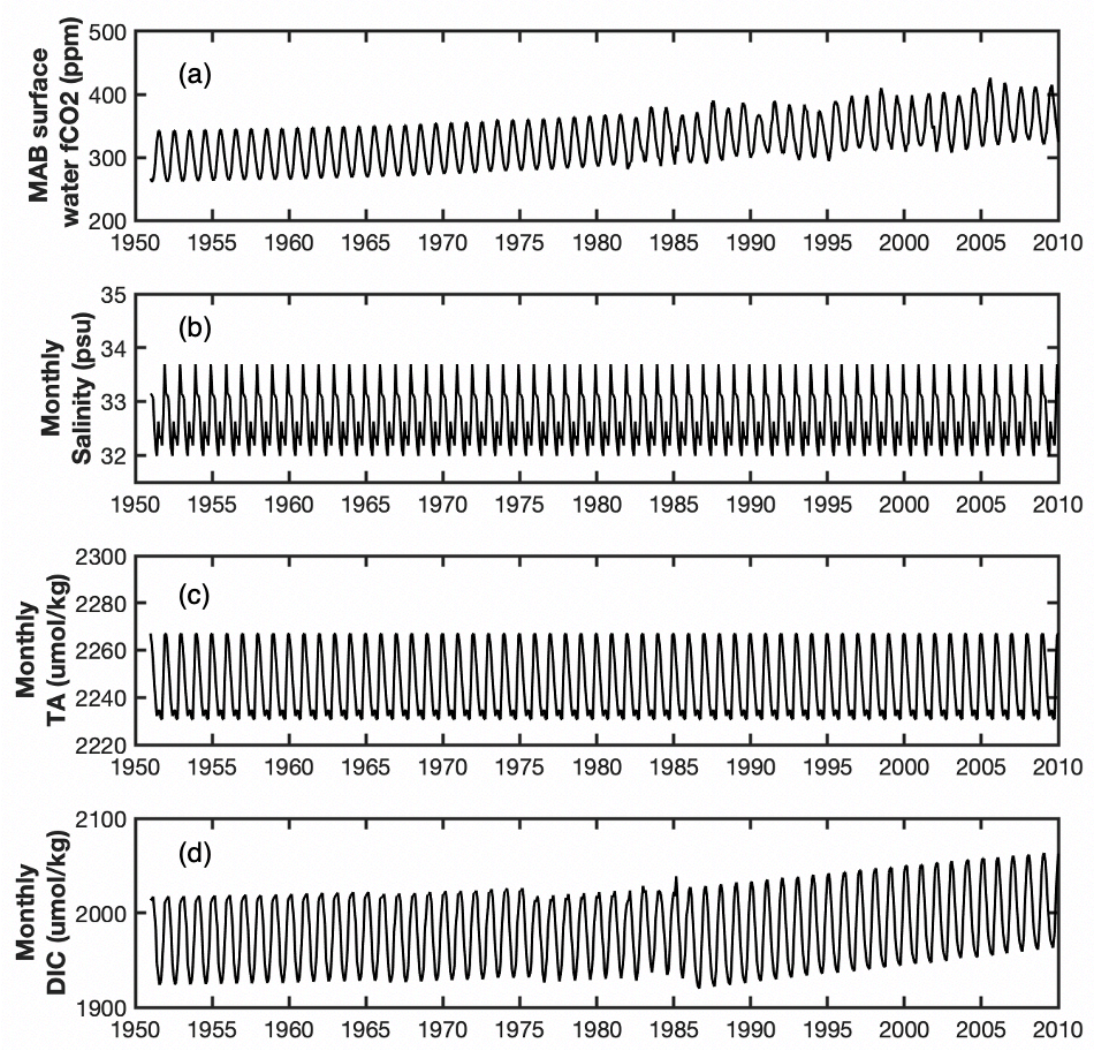

Figure 2.5 (a) Reconstructed sixty-years ocean boundary surface water fCO_2. (b) Sixty-years climatology ocean boundary salinity from WOA 2013 V2. (c) Calculated sixty-years ocean boundary TA. (d) Calculated sixty-years ocean boundary DIC.

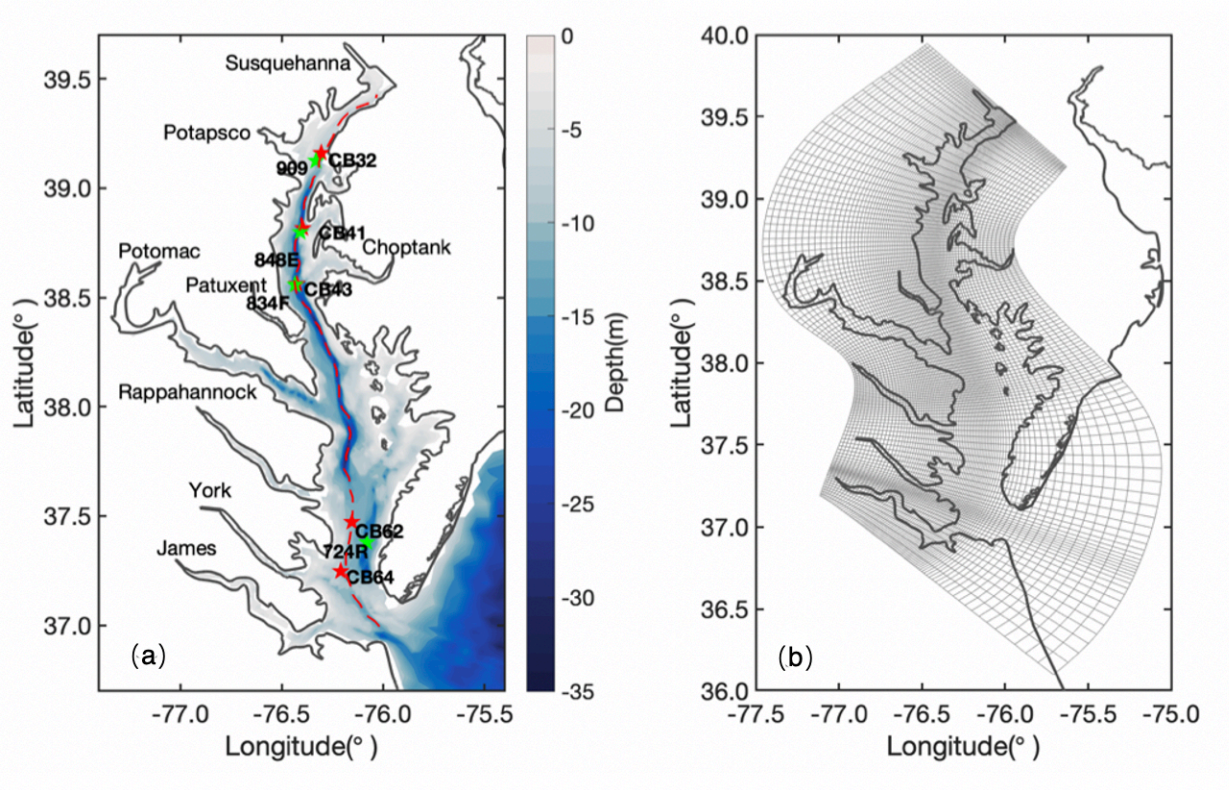

Figure 2.6. (a) Chesapeake Bay bathymetry. The dashed red line marks the along channel section and stars represent the stations where carbonate chemistry parameters are analyzed (red stars represent the Chesapeake Bay Program stations (data covering 1984-present); green stars represent Chesapeake Bay Institution stations (data covering 1949-1982). (b) The grids for the ROMS-RCA-CC models used in this research.

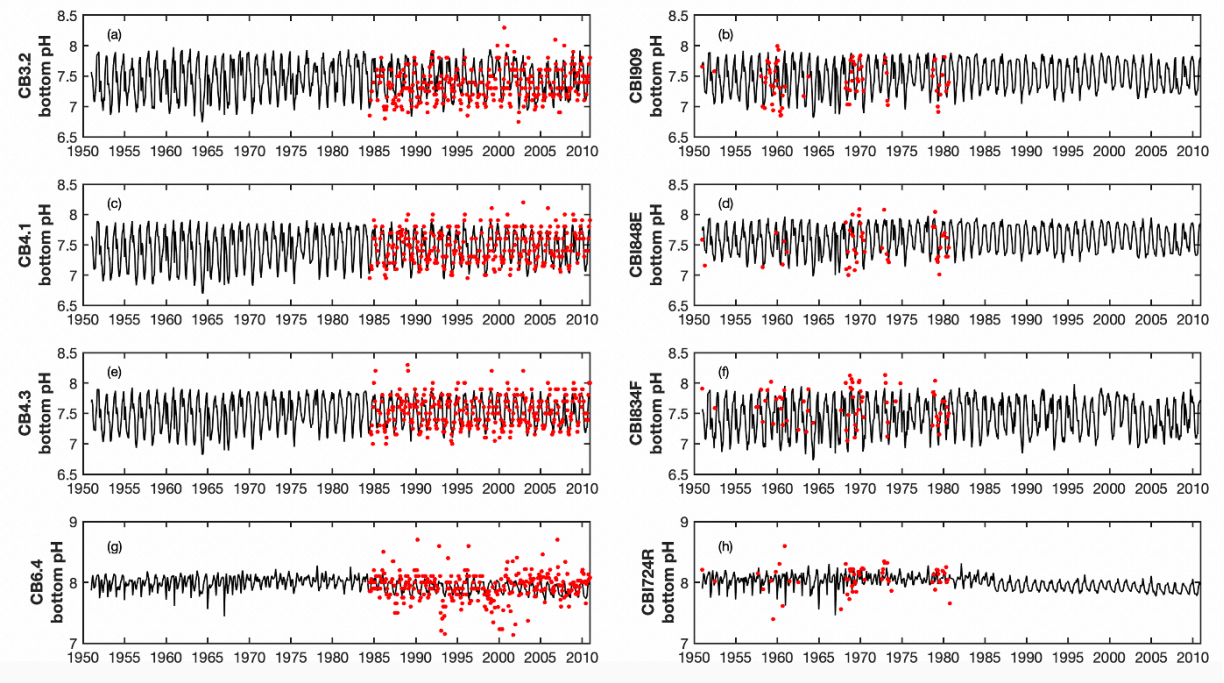

Figure 2.7. Model validation evaluation of bottom pH at CBP and CBI monitoring stations along central channel of main Chesapeake Bay (stations location see Figure 2.5). Red dots represent observation, black lines represent model results.

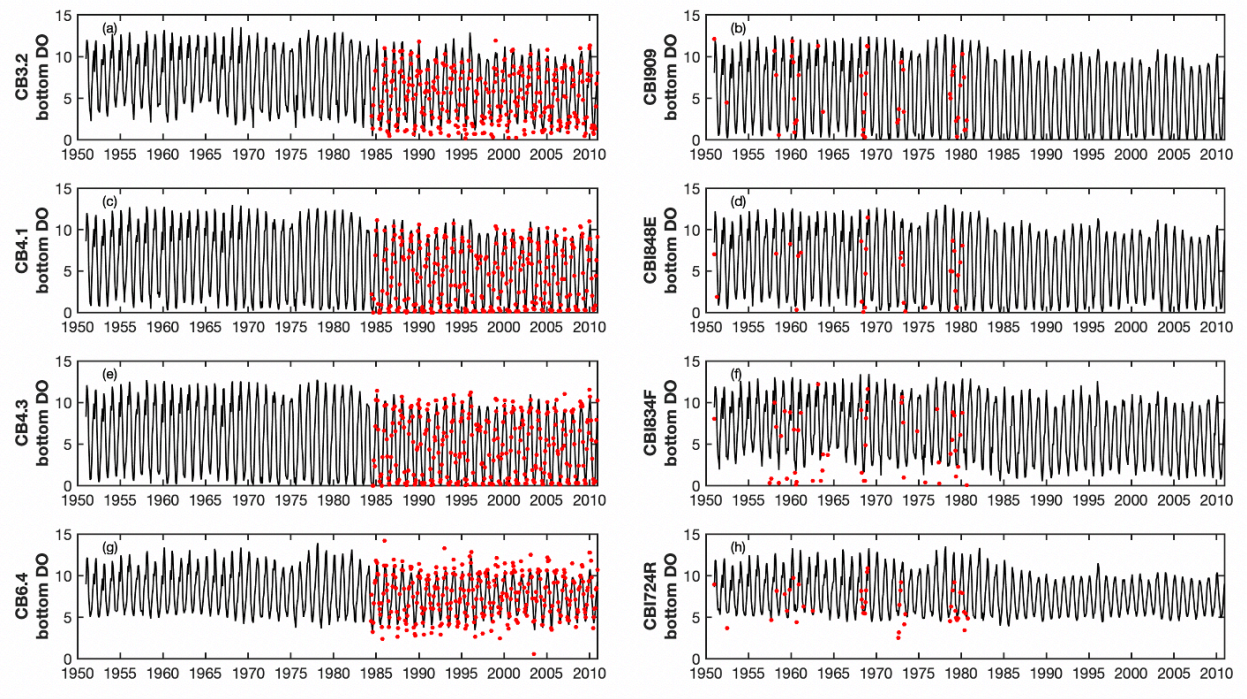

Figure 2.8 Model validation evaluation of bottom O_2 at CBP and CBI monitoring stations along central channel of main Chesapeake Bay (stations location see Figure 2.5). Red dots represent observation, black lines represent model results.

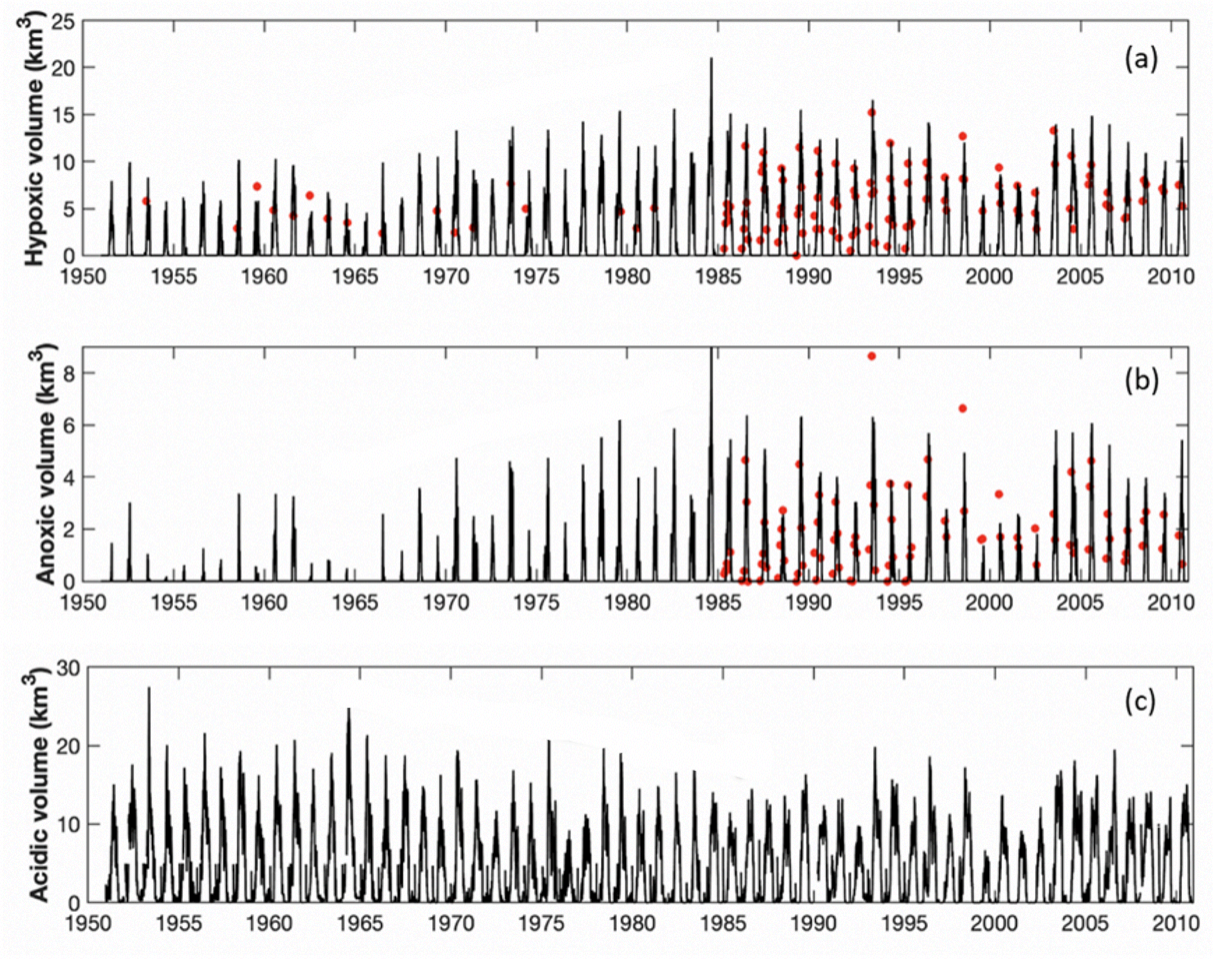

Figure 2.9. (a) Modeled hypoxic volume (O_2<2mg/L) in comparison with estimated hypoxic volume from observation data. (b) Modeled anoxic volume (O_2<0.5mg/L). (c) modeled acidic volume (pH<7.5). Model results were averaged at bi-week interval. Solid lines are modeled results, red dots are observations.

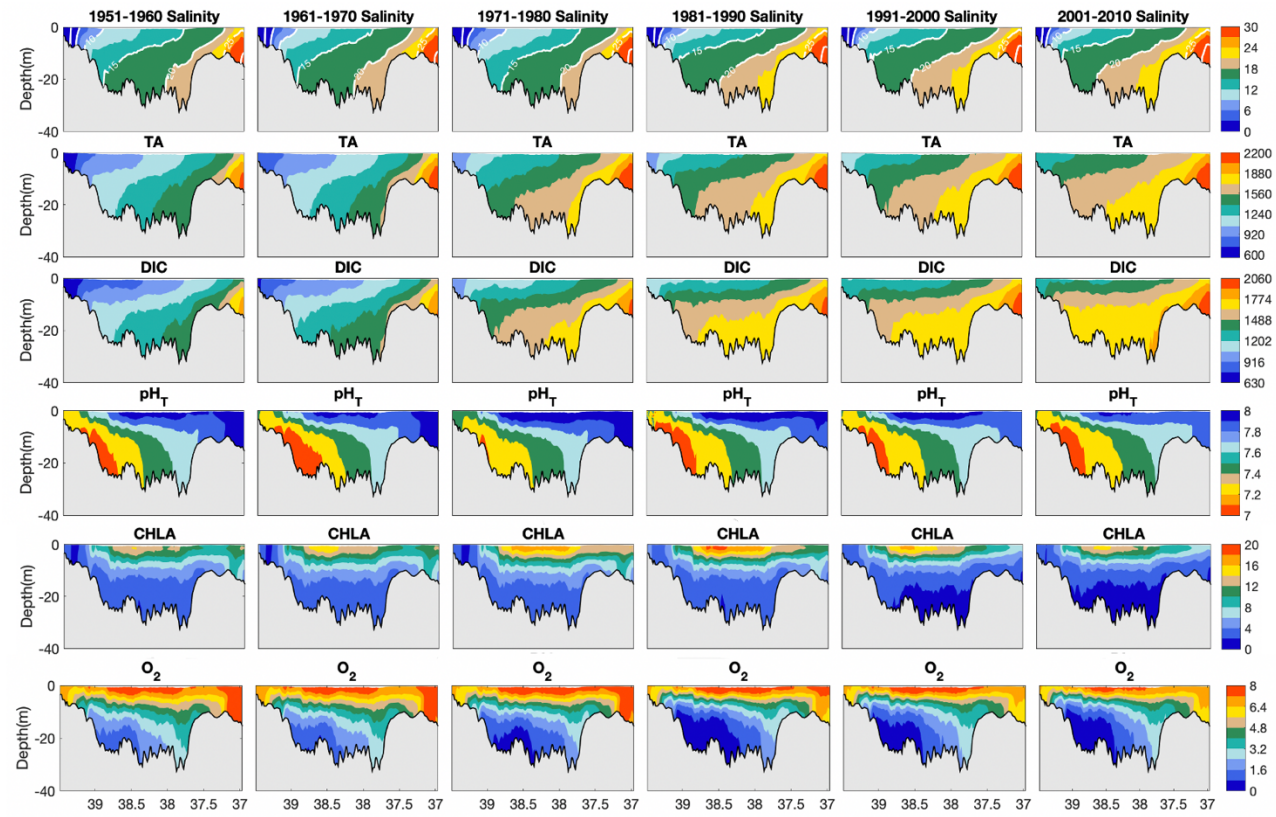

Figure 2.10. Modeled along-channel distribution of summer averaged salinity, TA, DIC, pH, Chlorophyll-a and O_2 in six decades (1950s, 1960s, 1970s, 1980s, 1990s and 2000s)

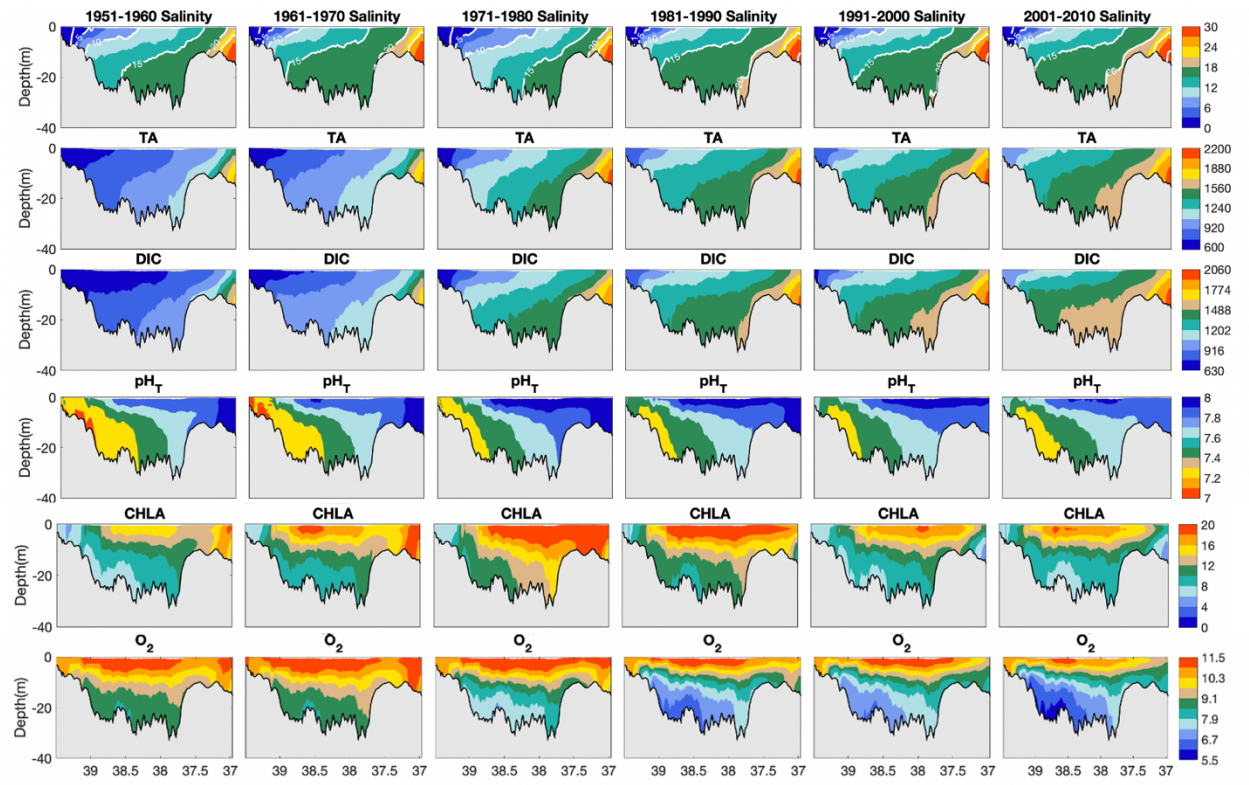

Figure 2.11. Modeled along-channel distribution of spring averaged salinity, TA, DIC, pH, Chlorophyll-a and O_2 in six decades (1950s, 1960s, 1970s, 1980s, 1990s and 2000s)

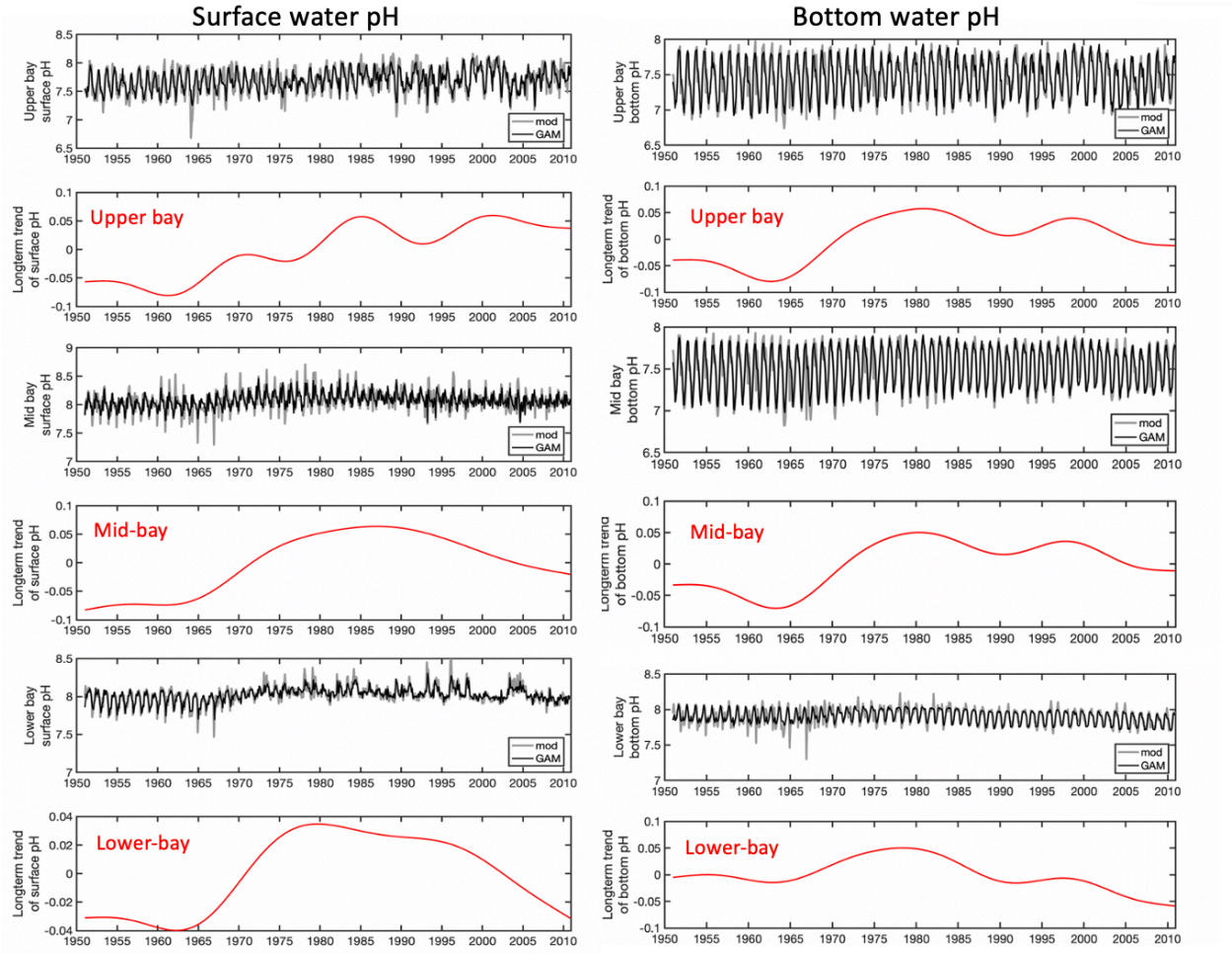

Figure 2.12 GAM fit on modeled surface and bottom pH at upper, mid and lower bay (upper panel). The long-term trend in GAM of modeled surface and bottom pH at three different sub-regions of Chesapeake Bay (lower panels).

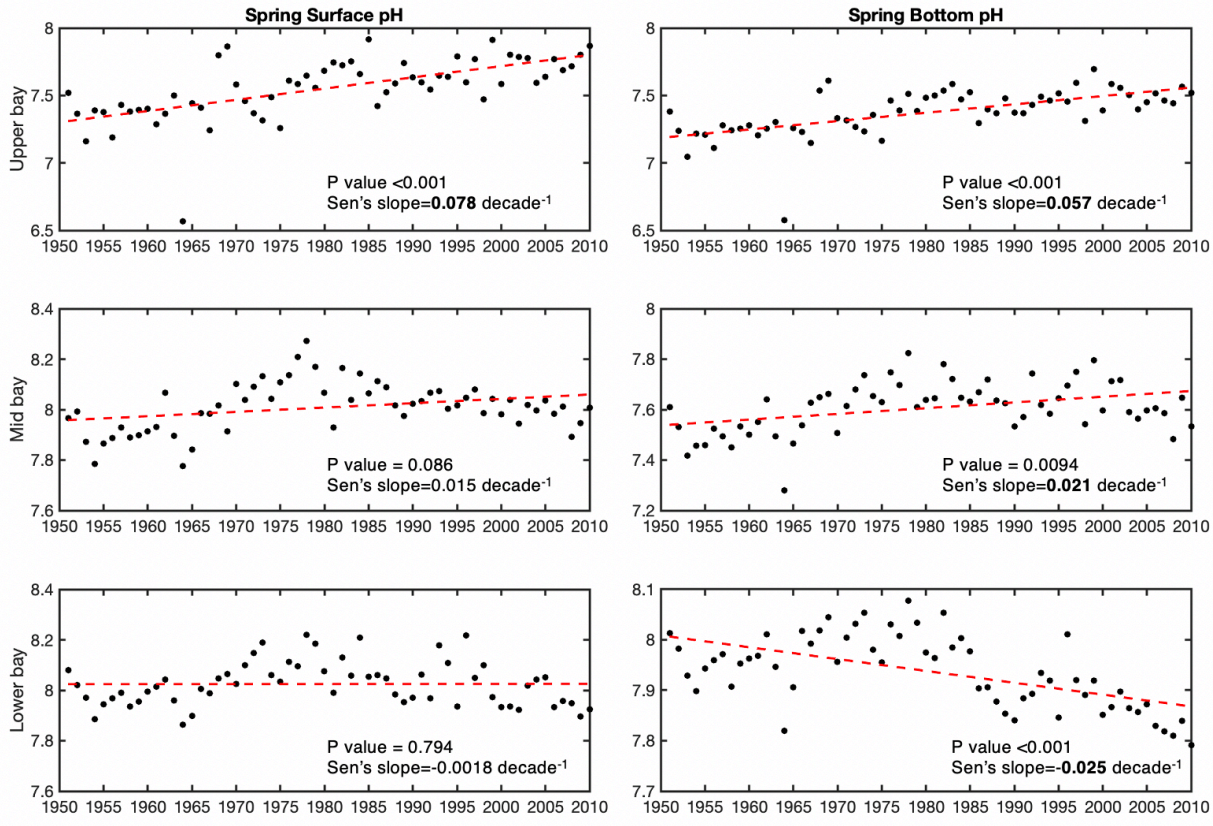

Figure 2.13 Spring averaged surface(left) and bottom(right) pH in upper, mid and lower bay. The Sen's slope in bold indicated the slope is statistically significant (p value< 0.05).

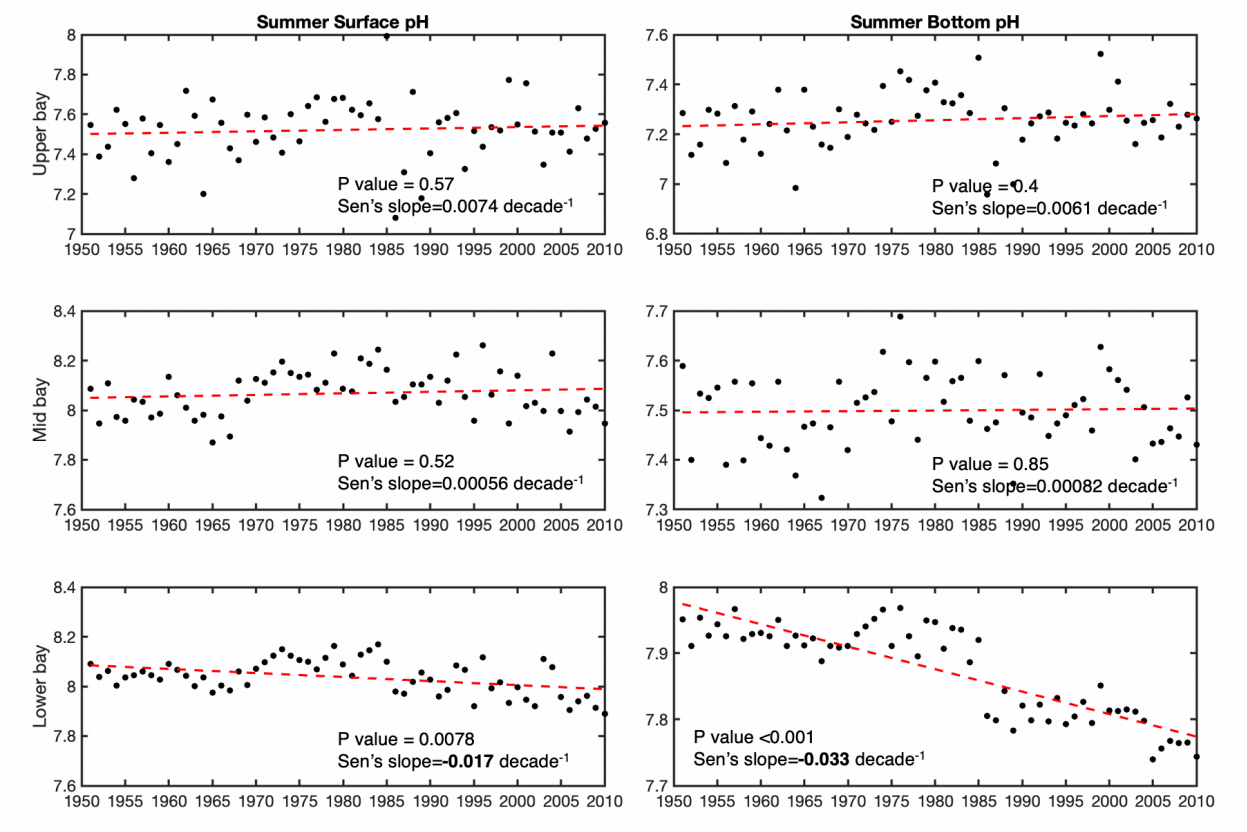

Figure 2.14. Summer averaged surface(left) and bottom(right) pH in upper, mid and lower bay. The Sen's slope in bold indicated the slope is statistically significant (p value< 0.05).

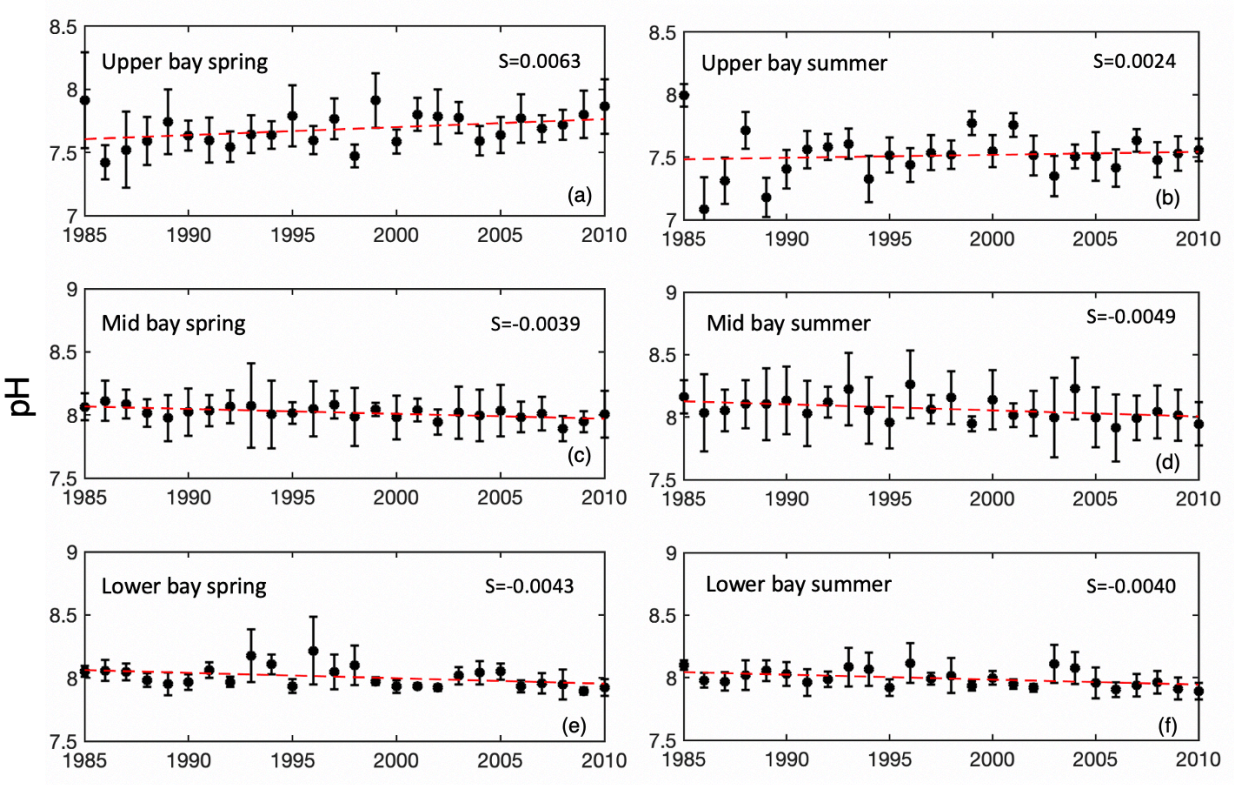

Figure 2.15. Modeled seasonal surface pH averaged in different subregion of the bay. Error bars represent 1 standard deviation. The dashed lines represent best linear fit. Symbol S represents slope of simulated values.

Table 2.1. Averaged DIC/TA ratio in 1986-2010 in seven tributaries from USGS observations.

	Patapsco	**Patuxent**	**Potomac**	**Rappahannock**
DIC/TA ratio	1.067	1.100	1.034	1.099
	York	**James**	**Choptank**	
DIC/TA ratio	1.098	1.097	1.230	

Table 2.2. Average summer hypoxic volume, accumulative hypoxic volume days, timing of onset, end and duration of hypoxia (threshold =0.5 km^3)

	Jun-Aug HV (km^3)	CHD (km^3days)	onset	end	duration
1950-1959	2.9	201	174	248	73
1960-1969	3.1	258	169	252	83
1970-1979	4.9	627	146	275	129
1980-1989	6.3	856	133	270	137
1990-2000	5.5	666	152	270	118
2001-2010	5.8	728	149	274	125

Table 2.3. Average summer acidic volume, accumulative acidic volume days, timing of onset, end and duration of acidification (threshold =0.5 km^3)

	Jun-Aug ACV (km^3)	CHD (km^3days)	onset	end	duration
1950-1959	9.22	1436	72	297	225
1960-1969	9.98	1616	76	277	201
1970-1979	7.95	1218	86	323	237
1980-1989	8.65	1128	94	286	192
1990-2000	8.74	1278	81	289	208
2001-2010	10.17	1272	86	284	198

Chapter 3: Scenario model runs to discern drivers of long-term pH trends in the Chesapeake Bay

3.1 Introduction

Ocean acidification due to the increasing emission of anthropogenic carbon into the atmosphere can cause open ocean pH to decrease at a rate of around 0.002 units per year (Doney et al. 2009, Hofmann et al. 2011, Carstensen and Duarte 2019). But the coastal and estuarine pH can have a much larger decreasing trend due to many local drivers (Borges and Gypens 2010, Provoost et al. 2010, Waldbusser et al. 2011, Carstensen and Duarte 2019). On the other hand, the water with high alkalinity exported from rivers (also called 'river Alkalinization') can increase the pH and aragonite saturation level in receiving estuarine and coastal waters. Kaushal et al. (2013) found 62 of the 97 sites in eastern US rivers had a significant long-term trend of increasing alkalinity. Both mining activities and chemical weathering could be attributed to this river alkalinization trend (Raymond and Oh 2009). Therefore, to understand the long-term pH trend in an estuarine system it is important to understand the trend of these local drivers and how they exert influence on pH.

Chesapeake Bay is the largest estuary in US and has long been suffered from eutrophication and hypoxia since 1950s (Hagy et al. 2004, Kemp et al. 2005a). But not only the hypoxia is sensitive to the changes in nutrient loading in Chesapeake Bay (Hagy et al. 2004), the elevated nutrients from riverine flow can also fuel the development of acidification in Chesapeake Bay by increaseing esturiane respiration (Shen et al., 2019). Long-term observations of alkalinity and pH in Susquehanna River, the major freshwater sources to Chesapeake Bay, revealed robust basification signals (Raymond and Oh 2009, Kaushal et al. 2013). These alkalinized waters from

tributaries can buffer the acidic oceanic water and increase the estuarine pH. Besides the riverine nutrients loads and river basification, climate change was also observed to affect Chesapeake Bay. The surface water temperature in the bay increased at the rate of 0.05 to 0.10 °C per year over the past 30 years (Ding and Elmore 2015), and the relative sea level rise in bay also accelerated in last century and reached 4-10 mm $year^{-1}$ in 2011 (Ezer and Corlett 2012). The warming temperature can alter the CO_2 gas exchange with the atmosphere and influence the metabolism process in bay. Sea-level rise can increase water column stratification and contribute to the decoupling of production and respiration in estuarine water. In summary, all these factors can have a different impact on Chesapeake Bay acidification. But how the individual factors can influence the long-term pH trend in bay is not well understood due to the limited observation coverage and the complexity of the estuarine ecosystem.

In this chapter, we analyzed long-term trends of the four main pH drivers in Chesapeake Bay (river basification, nutrient loading change, atmosphere CO_2 rising, warming and sea-level rise) using the GAM model and M-K trend analysis. Then based on the retrospective simulation in chapter 2, we removed these trends one-by-one in each of the scenario model runs to explore their individual impacts on long-term pH variations in Chesapeake Bay.

3.2 Method

Ocean acidification, river basification, riverine nutrient loading and climate change (warming and sea-level rise) are the four main drivers of the historical change in Chesapeake Bay acidification. To find out how these factors individually affected Chesapeake Bay acidification from 1951 to 2010, four scenario runs were conducted in which long-term trends in atmospheric pCO_2 (DtrpCO_2 run), riverine TA and pH (DtrBasi run), riverine nutrients (DtrNut run), temperature and off-shore water level (DtrTempslr run) were removed, respectively (Table 3.1).

The pCO_2 in the Mid Atlantic Bight (MAB) had an increasing rate of around 1.8 ppm per year from 1982 to 2015 due to anthropogenic CO_2 uptake (Xu et al. 2020). According to Equations (2.2) - (2.4), seawater fCO_2 increased 1.22 ppm per year (M-K $p<0.05$) from 1950 to 2010. To remove the long-term trend in seawater fCO_2, the increase rate of 1.22 ppm per year was subtracted from the annual average of the original time series. The new detrended fCO_2 equals to the sum of seasonal variation from the original fCO_2 and detrended annual averaged fCO_2 (Figure 3.1). M-K test was conducted and Theil-Sen slope was calculated from the detrended fCO_2 to ensure there was no statistically significant trend left. With the detrended fCO_2 and original off-shore TA, new ocean boundary DIC was calculated using CO2SYS code. And atmospheric CO_2 over the sixty year was also kept at the same level as 1951 in the ocean acidification detrend run.

Susquehanna TA and pH time series showed both large interannual and seasonal variation related to mining activities, mineral weathering and change of river discharge (Kaushal et al. 2018) (Figure 3.2). The long-term trend of TA and pH were calculated from the GAM fit model followed equation (2.1). Detrended TA and pH equals the original time series minus non-linear long-term trend detected through GAM fit model. New Susquehanna DIC was also calculated using CO2SYS using detrended TA and pH. M-K test was applied to both TA and pH to make sure no trend remained in the newly generated data.

The long-term trend of Susquehanna nutrients not only reflected the interannual changes of river flow but also nutrient management practices (Sprague et al. 2000, Zhang et al. 2015). Therefore, we used GAM fit model to extract non-linear long-term trend in Susquehanna nutrient time series. Since one of the major drivers of the acidification change in Chesapeake Bay is decoupling of primary production and respiration fueled by riverine inorganic nutrients, only the nitrate+nitrite (NO_{23}) and phosphate (PO_4) concentration from the Susquehanna River were

detrended (Figure 3.3). Detrended NO_{23} and PO_4 equal to the original time series minus non-linear long-term trend detected through GAM fit model. And no remaining increasing trend was detected through the M-K test.

Both temperature and ocean boundary sea level were detrended in climate change detrend scenario run (DtrTempslr). Air temperature over Chesapeake Bay and the riverine temperature in the tributaries have increased over the past several decades (Rice and Jastram 2015, Ding and Elmore 2015). The riverine temperature influences the estuarine temperature through river inflows while the air temperature affects it through the air-sea heat fluxes. To remove the long-term trends in temperature forcing, Mann-Kendall trend test (M-K test) was applied to the temperature time series at the upstream boundary of the eight major tributaries as well as the heat flux-related variables (air temperature, humidity, solar radiations) at NARR grids over Chesapeake Bay:

$$\mathrm{T_{detrend}} = \mathrm{T_{original}} - \mathrm{Slope_T} \times (\mathrm{Time} - \ 1/1/1951) \qquad (3.1)$$

where $T_{original}$ represents the original time series of each variable (including river temperature, surface air temperature, humidity, downwelling long-wave radiation and net short wave radiation), $T_{detrend}$ represents the detrended variables. $Slope_T$ is the Theil-Sen slope calculated from the original data. Equation (3.1) was only applied to the grids or tributaries when the p-value of M-K test was less than 0.4.

To remove the sea level rise, we removed the linear trend of the observed de-tided sea level time series at Duck, North Carolina. The detrended non-tidal sea level component was then added to the tidal sea level to produce the sea level time series at the offshore boundary:

$$\mathrm{SL_{detrend}} = \mathrm{H_{Duck}} - \mathrm{Slope_H} \times (\mathrm{Time} - \ 1/1/1951) \ + \ \mathrm{SL_{tide}} \qquad (3.2)$$

where H_{Duck} represents the de-tided sea level time series at Duck, $Slope_H$ is the Theil-Sen slope obtained from the de-tided time series at Duck, SL_{tide} is the tidal sea level and $SL_{detrend}$ represents the detrended sea level (Figure 3.4). And no remaining increasing trend was detected through M-K test.

3.3 Results

3.3.1 long-term pH trend analysis under different model scenarios

To discern the roles of rising atmosphere CO_2, river basification, river nutrient loading change and climate change (warming and sea-level rise) in driving the long-term trends in acidification in Chesapeake Bay, we analyzed the four scenario runs DtrpCO_2, DtrBasi, DtrNut and DtrTempslr and compared them with the hindcast run.

The long-term residual (*s(dnum)* from equation 2.1) in the GAM fit model to regionally averaged pH under different scenarios is shown in Figure 3.5. In general, surface and bottom pH showed overall similar trend over the sixty years. But different pH trends were detected in different regions.

In the upper bay, hindcast model results show surface water pH increased by around 0.1 with little fluctuation over the sixty years. (1) The DtrBasi run had the largest difference from other runs. This suggests if we had removed the river basification signal from the Susquehanna River, upper bay pH would have decreased around 0.3 in both surface and bottom pH. In other words, increasing riverine TA and pH observed in the Susquehanna River may be the largest driver that increased upper bay pH for both surface and bottom water. (2) The long-term pH trends among DtrpCO_2, DtrNut and Dtrtempslr scenario runs were similar. Their pH also increased by around 0.1 over the sixty years like the hindcast pH but experienced more fluctuations. It indicates that,

atmospheric pCO_2 rising, riverine nutrient loading or global climate change had relatively small influence on upper bay pH compared to river basification. But without their influences, upper bay pH would have larger increasing rate before 1985.

In the mid bay, hindcast model results show pH first increased from 1950s to 1980s then slightly decreased after 1980s in both surface and bottom water. The overall pH increased around 0.05 in surface water and increased around 0.01 in bottom water in the sixty years. (1) Like the upper bay, the DtrBasi run also had the largest pH difference from other runs in mid bay water. The DtrBasi result shows river basification had big influence in increasing surface and bottom pH. Without the river basification, mid bay pH would decrease around 0.1 for surface water and 0.18 for bottom water. (2) DtrpCO_2 pH had the second largest difference from other runs. Without the atmospheric pCO_2 rising, surface and bottom pH would have larger increase rate in the sixty years. (3) Riverine nutrient loading and global climate change had the smallest influence on mid bay pH compared to previous two drivers.

In the lower bay, hindcast pH showed an overall decrease of 0.03 in the surface water and a decrease of 0.08 in the bottom water from 1951 to 2010. Both DtrBasi and DtrpCO_2 had large pH difference compared to other scenario runs. (1) The DtrpCO_2 run result shows without atmospheric pCO_2 rising, surface and bottom pH would both increase but surface pH would have bigger increase rate. (2) DtrBasi run result shows river basification still had big impact increasing the pH even in the lower bay. Without river basification, lower bay surface and bottom pH would both decrease. (3) Nutrient loading from rivers and climate change had small impact on lower bay pH change.

Then we took a closer look at the seasonal average pH in different subregions of the bay under different scenarios and compared the trends with the hindcast results. To do this, we

calculated the summer and spring average pH and chlorophyll-a because acidification in the Chesapeake Bay usually starts in spring and ends in late summer (Table 2.3). Chlorophyll-a is a commonly used estimator for the phytoplankton biomass amount. The spring phytoplankton bloom can increase the surface pH by consuming CO_2 from water. But after the spring bloom, more organic matter sinks to the bottom of the water, and the increased organic matter respiration can further lower the bottom pH during summer. We calculated the seasonal averaged surface chlorophyll-a to help us find out whether the surface pH change closely relates to surface phytoplankton growth from 1951 to 2010.

The overall seasonal pH trend differences in different scenario runs agree with what we get from the GAM fit residuals in Figure 3.5. In the upper bay (Figure 3.6), river basification was the largest driver that controls and increases both surface and bottom pH. Climate change including warming and sea-level rise would decrease upper bay chlorophyll-a concentration during summer after the 1980s. But this decrease did not have detectable influence on upper bay summer pH. In the mid bay (Figure 3.7), river basification was still the largest driver increasing mid bay pH but the rising pCO_2 started to have bigger impact decreasing the pH. It is worth noticing that the increasing riverine nutrient loading in the 1970s and 1980s played an important role in increasing the mid bay spring chlorophyll-a which agrees with the development of eutrophication in Chesapeake Bay observed in previous studies (Kemp et al. 2005a). But this change in phytoplankton biomass had relatively smaller impact on pH compared to atmospheric pCO_2 rising and river basification. In the lower bay (Figure 3.7), atmospheric CO_2 rising had a bigger influence in decreasing surface and bottom pH compared to mid and upper bay. River basification and rising atmospheric pCO_2 became equally important in controlling lower bay water pH.

3.3.2 Acidic and hypoxic volumes under different model scenarios

Another way to analyze how these drivers changed the Chesapeake Bay acidification is by comparing the decadal averaged acid volumes and the onset (break up) timing of the acidification events under different scenarios. Hypoxic volume was also calculated during the analysis.

In Figure 3.9, the decadal average acidic volumes in hindcast run showed different trends in different months. The acidic volume in August showed an overall increasing trend, but the acidic volumes in June and July showed more fluctuations. Acidic volume in the DtrBasi scenario run showed the largest difference with the hindcast run compared to other scenario runs. The result shows river basification would decrease the summer acidic volume by an average of 44.5% by the 2000s. The second largest driver of acidic volume change was the rising atmospheric pCO_2, which would increase the summer acidic volume by an average of 14.2% by the 2010s. What is worth mentioning is that warming and sea-level rise had the opposite influence on acidic volume in early and late summer. In June, climate change decreased the acidic volume by around 16.9% by the end of the 2000s. But in August, climate change increased the acidic volume by around 19.4% by 2010. The fourth main driver is riverine nutrient loading, which would decrease 6.8% of the total acidic volume change during summer by the 2000s.

Hypoxic volume showed a more obvious increasing trend in all three months, especially from the 1950s to 1980s, compared to the acidic volume, then it stabilized after 1990, which agrees with the observation from Haggy et al. (2004) (Figure 3.10). Detrend of atmospheric pCO_2 or river basification cannot have influence on hypoxic volume. But detrending riverine nutrient loading and climate change can decrease the summer hypoxic volume by 9.7% and 26.0% respectively.

Then we used the mid-Bay station CB4.3 as an example to calculate onset and break up timing of the acidification and hypoxia in Chesapeake Bay under different scenarios. For acidification, we calculated the day of a year when CB4.3 bottom pH first fell below 7.5 (T_{acid_ini}) in spring and the day of a year when pH rose above 7.5 (T_{acid_end}) in late summer. For hypoxia, we calculated the day of a year when O_2 first fell below 2 mg/L (T_{hyp_ini}) in spring and the day of a year when O_2 rose above 2 mg/L (T_{hyp_end}) in fall (Figure 3.13). M-K test and Sen's slope were also calculated to detect the long-term trend of the onset and break up timings.

For acidification, the onset timing mostly occurred in April, but it has a large variation spanning from early March to late May (Figure 3.11). The M-K test showed that there was no significant long-term trend in the hindcast run. And there was no long-term trend in DtrBasi, DtrNut or Dtrtempslr either. But in DtrpCO_2, an upward trend with Sen's slope of 6.7 days/decade is detected. It suggests that T_{acid_ini} would have been delayed by around 40 days without rising atmospheric pCO_2 over the past six decades. We also calculated the difference in the acidification initiation day ΔT_{acid_ini} between the four scenario runs and the hindcast run (Figure3.11 (c)). ΔT_{acid_ini} was nearly zero in DtrNut run, indicative of no influence from nutrient loading change. ΔT_{acid_ini} was slightly positive in Dtrtempslr run in most of years (up to 20 days in 1977 and 2002) but with an outlier of -50 days in 1976, suggesting that warming and sea-level rise could in general make acidification initiation earlier over the sixty years. Rising atmospheric pCO_2 did not have big impact on acidification initiation day until 1990s. After 1990s, ΔT_{acid_ini} in DtrpCO_2 increased and reached 50 days in mid 2000s with a maximum of 75 days in 2009. The averaged ΔT_{acid_ini} in DtrBasi run was biggest among all the scenario runs. The largest ΔT_{acid_ini} in DtrBasi reached up to -50 days in early 1950s, mid 1970s and 2000s when Susquehanna river flow was larger than

normal years (Kemp et al. 2005a). It suggests that river basification can delay the acidification by 50 days in wet years.

The termination of acidification mostly happened in August. The M-K test shows that T_{acid_end} shifted later in hindcast run and all the scenario runs. In hindcast run, T_{acid_end} delayed 15 days from 1951 to 2010 at a rate of 2.5 days/decade. Among all the upward T_{acid_end} trends detected in different scenario runs, DtrBasi and Dtrtempslr had the largest slope of 4.0 days/decade and 3.2 days/decade. It means T_{acid_end} would have been delayed by around 24 days or 19 days without river basification or climate change (warming and sea-level rise) over the past six decades. The results can be clearly shown in ΔT_{acid_end} plot (Figure3.11 (d)). The T_{acid_end} in both DtrpCO_2 and DtrNut were nearly zero before 1970s, indicative of no influence from nutrient loading change and pCO_2 rising before 1970s. Since mid 1970s, ΔT_{acid_end} in DtrNut and DtrpCO_2 turned negative. ΔT_{acid_end} in DtrpCO_2 varied around -10 days. ΔT_{acid_end} in DtrNut was in general under -10 days but with outliers of -35 and -28 in 1975 and 2003. It suggests nutrient loading change had less influence on acidification termination than rising atmospheric pCO_2 although both drove a later termination by several days. ΔT_{acid_end} in DtrBasi and Dtrtempslr was positive, and their absolute values were larger than other two scenario runs. The maximum ΔT_{acid_end} in DtrBasi and Dtrtempslr reached up to 19 days and 25 days respectively after 1990. It suggests river basification and climate change can both bring acidification termination earlier in late summer and they had bigger influence on acidification termination than pCO_2 rising or nutrient loading change.

For hypoxia, the initiation time (T_{hyp_ini}) mostly occurred in June. It first decreased from 1950 to 1980 then gradually increased after 1980 (Figure 3.12). The M-K trend test shows that the overall hindcast T_{hyp_ini} has a decreasing trend of -3.1 days/decade. From 1950 to 2010, the hindcast hypoxia initiation time got earlier by around 18 days. T_{hyp_ini} in DtrNut and Dtrtempslr has

relatively smaller decreasing trend than hindcast run. The result indicates T_{hyp_ini} would have been earlier by around 15 days or 14 days without nutrient loading change or climate change over the past six decades. The overall hypoxia termination time (T_{hyp_end}) was increasing. The M-K test showed hindcast T_{hyp_end} delayed around 23 days at the rate of 3.9 days/decade from 1951 to 2010. Without nutrient loading or climate change, T_{hyp_end} increase can have slowed down to 3.8 days/decade or 3.6 days/decade respectively. The ΔT_{hyp_end} plot shows climate change had overall larger impact on delaying T_{hyp_end} than nutrient loading change. River basification and atmospheric pCO_2 rising had no influence on hypoxia initiation or termination.

3.4 Conclusion and discussion

In this chapter, we used the coupled hydrodynamic-biogeochemical-carbonate chemistry (ROMS-RCA-CC) model to conducted additional numerical experiments in which we removed trends in each long-term driver to discern the separate effects of river basification, atmospheric pCO_2 rising, riverine nutrient loading change, and climate change (sea level rise and warming).

Surprisingly, we found river basification to be the dominant forcing driving the long-term change of pH in the Chesapeake Bay in upper, mid, and even lower bay. Through the Monte Carlo trend analysis on Susquehanna River TA and pH historical observations, we detected an increasing rate of 10.43 μmol/kg per year and 0.014 units per year in TA and pH respectively which is consistent with previous observations (Raymond and Oh 2009, Kaushal et al. 2013). After removing this trend in DtrBasi, we found upper bay surface and bottom pH would decrease by roughly 0.3 units from 1951 to 2010 while the hindcast shows an increase by 0.1 units. In the mid bay, river basification was still the largest pH driver compared with other forcings. The surface water would have decreased by 0.1 unit and bottom water decreased by 0.18 unit if without its

signal. In the lower bay, river basification had smaller control on pH variation, but its impact was still obvious even compared to ocean acidification through riverine water export. By analyzing the acid volume and its initiation and termination time under different scenarios, we found river basification would decrease the summer acidic volume by an average of 44.5% by the 2000s and shorten the acidification duration by one and half month with both later onset and earlier termination of about three weeks.

Ocean acidification seems to be the second dominant forcing that controlled the long-term acidification in the Chesapeake Bay. We found ocean acidification had relatively small influence on upper bay pH compared to river basification, but it had bigger impact decreasing pH in mid and lower bay. The rising atmospheric CO_2 can increase the summer acidic volume by roughly 14.2%. And by the end of 2000s, it can prolong the acidification duration by around two months with earlier initiation of 50 days and later termination of 10 days.

Nutrient loading change and climate change (sea level rise and warming) had relatively smaller impact on Chesapeake Bay acidification compared to the previous two factors. The DtrNut and DtrTempslr show that, without their influences, upper bay pH would have larger increasing rate before 1985. The increasing riverine nutrient loading in the 1970s and 1980s played an important role in increasing the mid bay spring chlorophyll-a which agrees with the development of eutrophication in Chesapeake Bay observed in previous studies (Kemp et al. 2005a). But this change in phytoplankton biomass had relatively smaller impact on pH compared to atmospheric pCO_2 rising and river basification. Both nutrient loading and climate change had nearly no impact on initiation time. But they had different impacts on acidification termination. Nutrient loading change can drive a later termination by less than 10 days (with outliers of -35 and -28 in 1975 and 2003). Warming and sea-level rise can bring acidification termination earlier up to 25 days in late

summer after 1990. However, in the DtrNut run the detrended nutrient loading still had large interannual variation (Figure 3.2 and Figure 3.3) which probably led to the fluctuation remained in the mid bay pH.

The main finding in this section is that river basification and rising atmospheric pCO_2 are the two largest drivers that control bay-wide acidification. And the increasing alkalinized water export from the Susquehanna River not only compensated CO_2-induced acidification but also decreased Chesapeake Bay acidification in terms of total acidic volume and duration. Previous studies found similar basification trend in other coastal systems. For example, research found an increasing export of alkalinized water from the Mississippi River which could be related to the increasing water discharge and agricultural land cover change (Raymond and Cole 2003, Raymond et al. 2008, Kaushal et al. 2018). And the basification trend was also observed in the Central Baltic Sea and Gulf of Bothnia which has compensated local CO_2-induced acidification by almost 50% and 100%, respectively (Müller et al. 2016).

This chapter is a general estimation of local and global impacts on Chesapeake Bay acidification from 1951 to 2010. The results highlight the great impact of riverine basification on bay-wide pH trends and the complex interactions among the local and global drivers on long-term pH trend over the sixty years. More work is necessary to investigate the detailed mechanisms of the individual impact from different pH drivers.

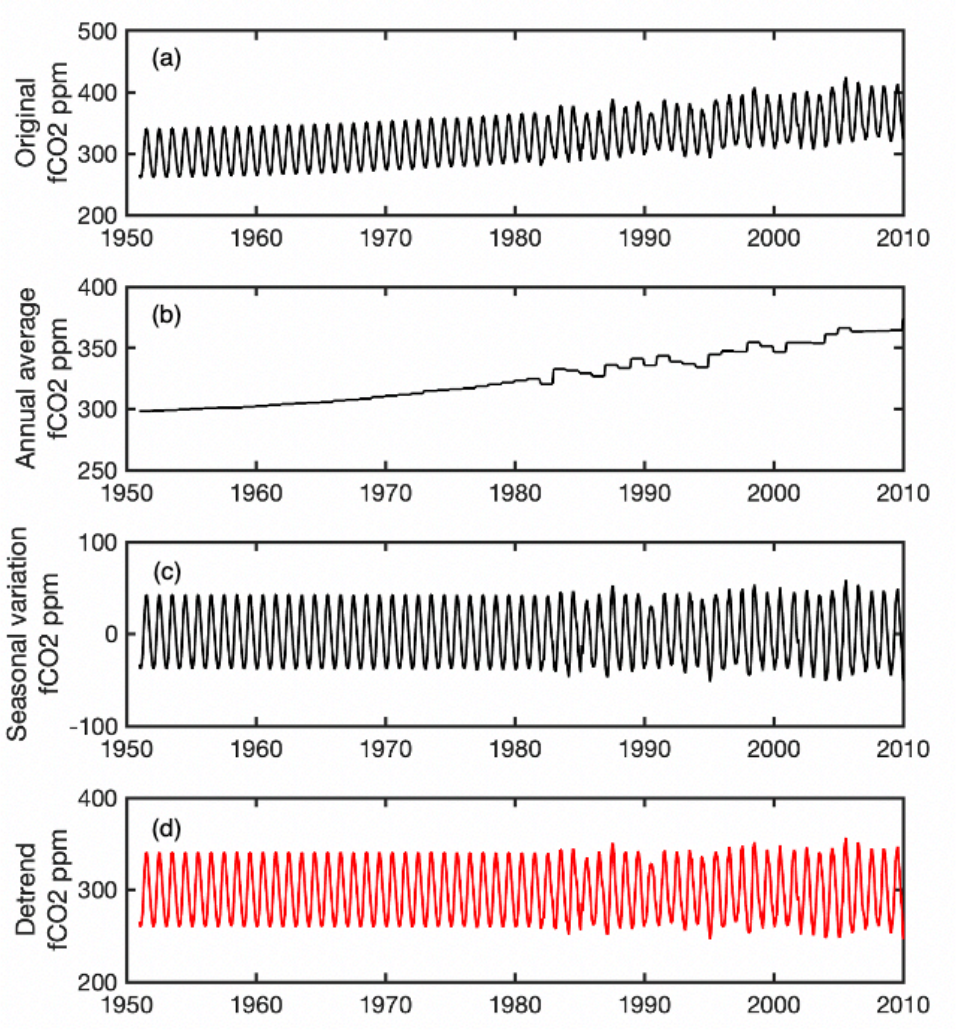

Figure 3.1 (a) Time series of surface water fCO_2 in hindcast run (b) annual averaged fCO_2 (c) fCO_2 seasonal variation (d) Detrended surface water fCO_2

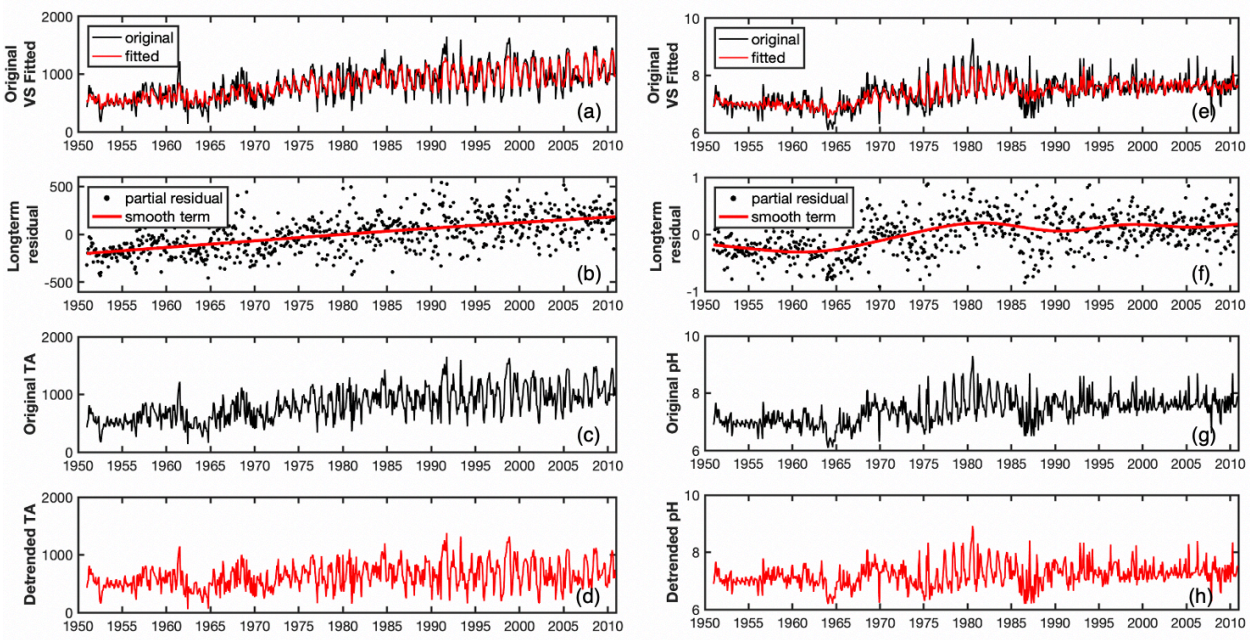

Figure 3.2 Time series of monthly (black line) and GAM fitted (red line) Susquehanna (a) TA (b) pH. (b)(f) Long-term TA, pH residuals (black dots) and their linear trends (red line) (c)(g) TA and pH from hindcast run (d)(h) Detrended TA and pH in DtrBasi scenario run

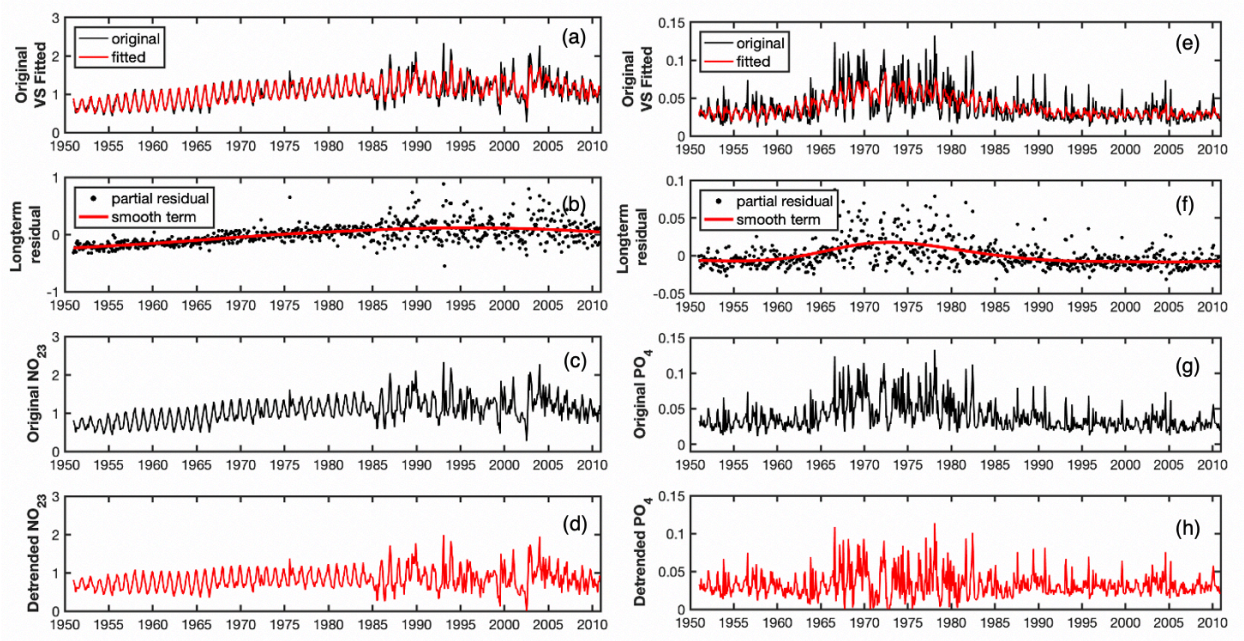

Figure 3.3 Time series of monthly (black line) and GAM fitted (red line) Susquehanna (a) Nitrate+Nitrite (NO_{23}) (b) Total phosphate (PO_4) (b)(f) Long-term NO_{23}, PO_4 residuals (black dots) and their linear trends (red line) (c)(g) NO_{23} and PO_4 from hindcast run (d)(h) Detrended NO_{23} and PO_4 in DtrNut scenario run

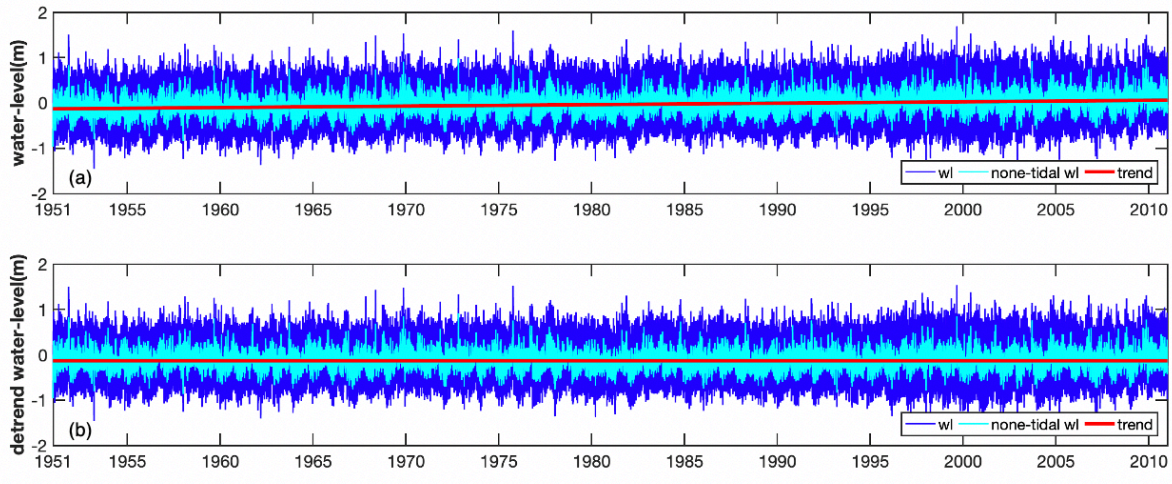

Figure 3.4 (a)Time series of water level of Duck, North Carolina used to force the ROMS model. The blue line shows the hourly observations, the cyan line shows de-tided water-level and the red line is the linear trend. (b) Detrended time series of water level.

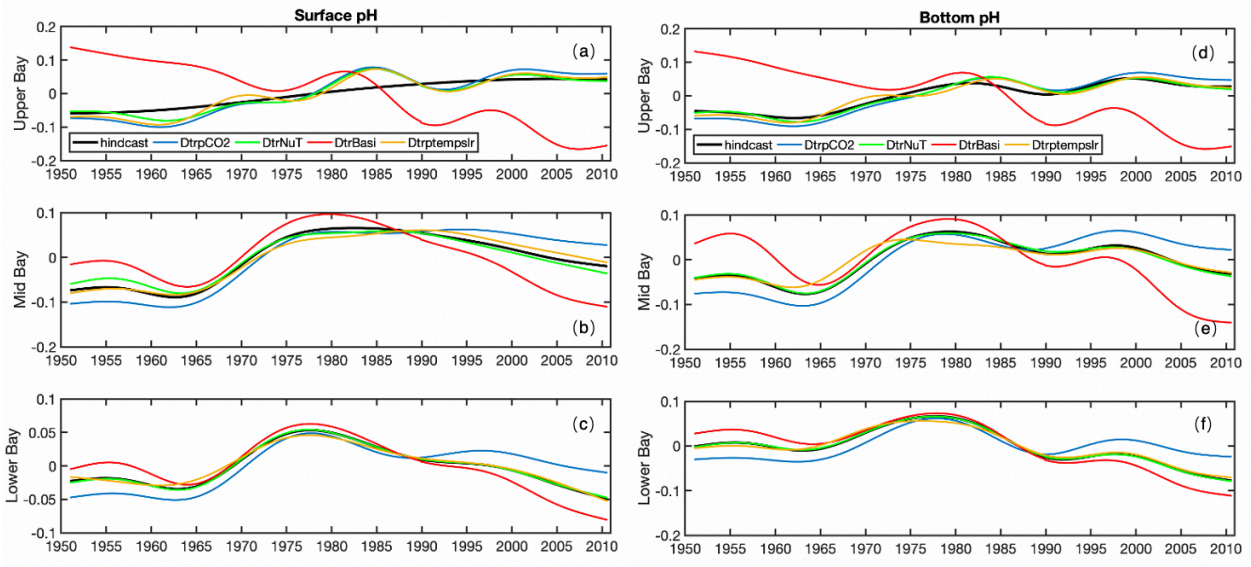

Figure 3.5. The long-term trend in GAM of modeled surface (a)(b)(c) and bottom pH (a)(b)(c) at three different sub-regions of Chesapeake Bay from hindcast and four scenario runs.

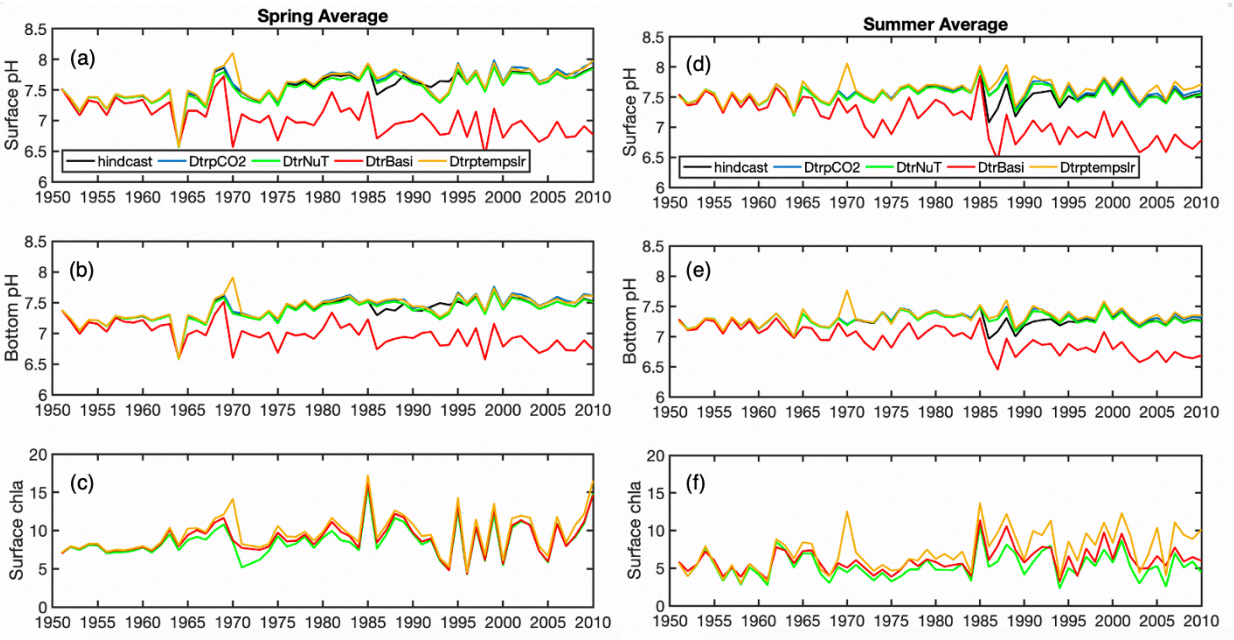

Figure 3.6. The spring averaged surface pH (a), bottom pH (b) and surface chlorophyll-a (c) and summer averaged surface pH (d), bottom pH (e) and surface chlorophyll-a (f) in the upper bay.

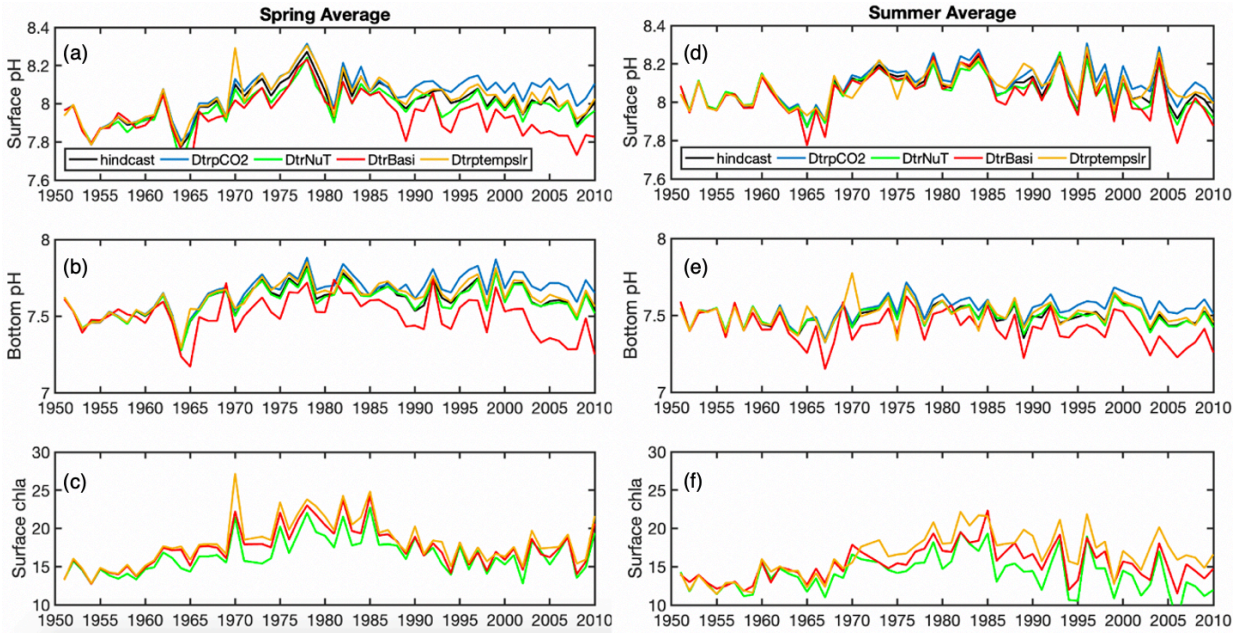

Figure 3.7. The spring averaged surface pH (a), bottom pH (b) and surface chlorophyll-a (c) and summer averaged surface pH (d), bottom pH (e) and surface chlorophyll-a (f) in the mid bay.

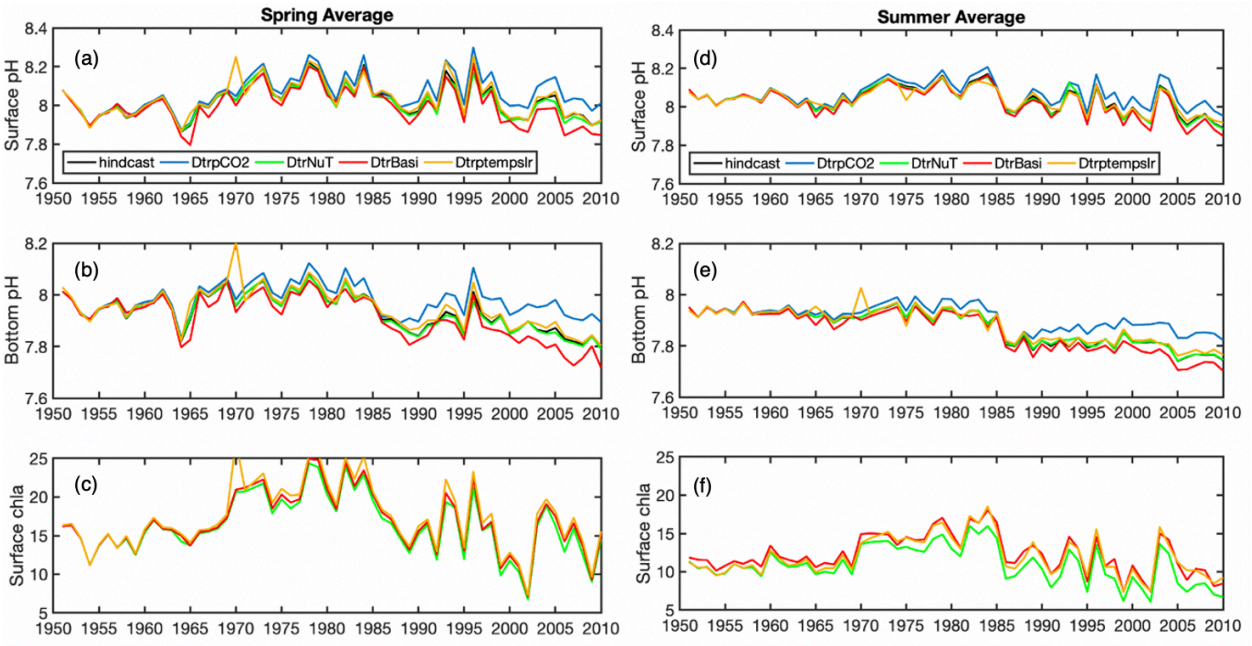

Figure 3.8. The spring averaged surface pH (a), bottom pH (b) and surface chlorophyll-a (c) and summer averaged surface pH(d), bottom pH (e) and surface chlorophyll-a (f) in the lower bay

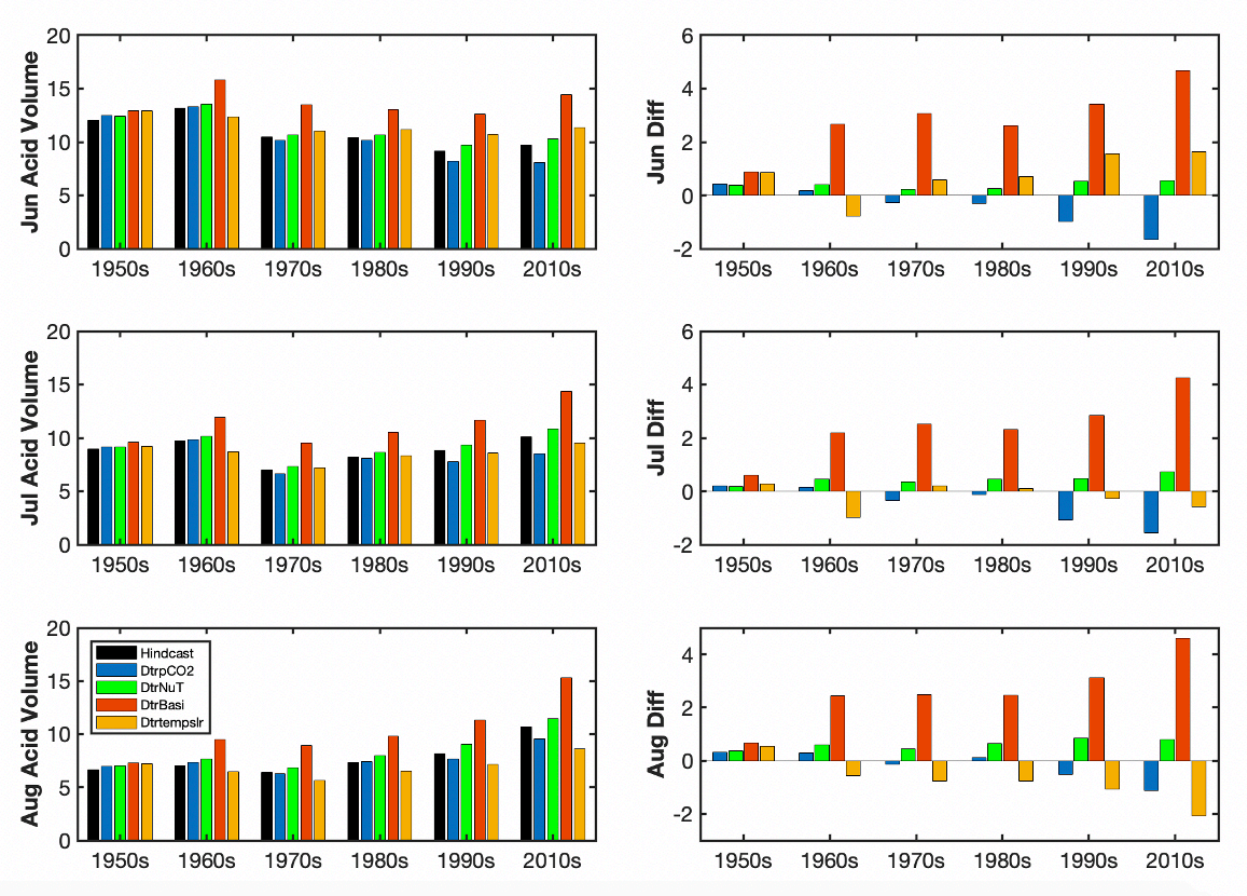

Figure 3.9. Acidic volume in Jun(a), July(b) and August(c); The difference between scenario run acidic volume and hindcast acidic volume in Jun (a), Jul(b) and August(c).

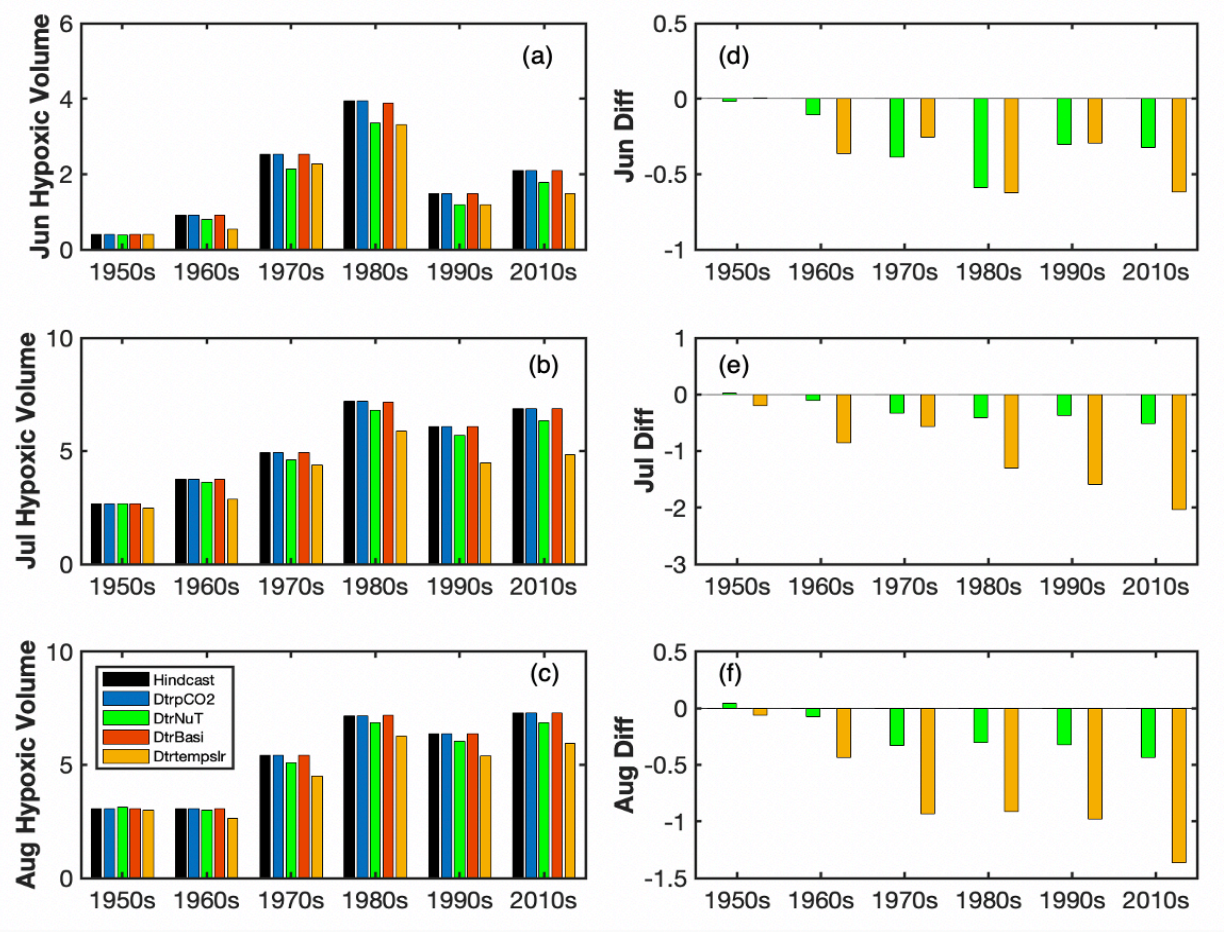

Figure 3.10. Hypoxic volume in Jun(a), July(b) and August(c); The difference between scenario run hypoxic volume and hindcast hypoxic volume in Jun (a), Jul(b) and August(c).

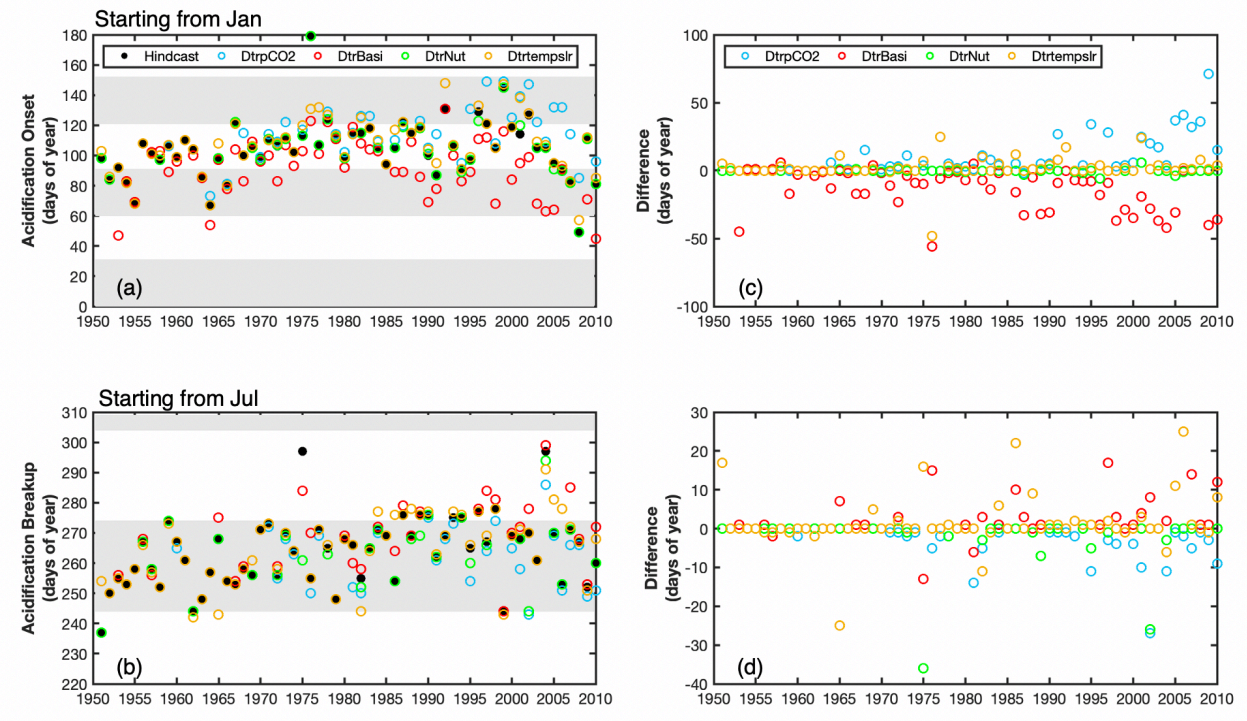

Figure 3.11 Acidification onset (a) and breakup (b) timing at CB4.3 from 1951 to 2010 by Hindcast run and four scenario runs. The difference of acidification onset (c) and breakup (d) timing between $DtrpCO_2$, DtrBasi, DtrNut, Dtrtempslr and Hindcast run correspondingly. The gray and white bars indicate different months.

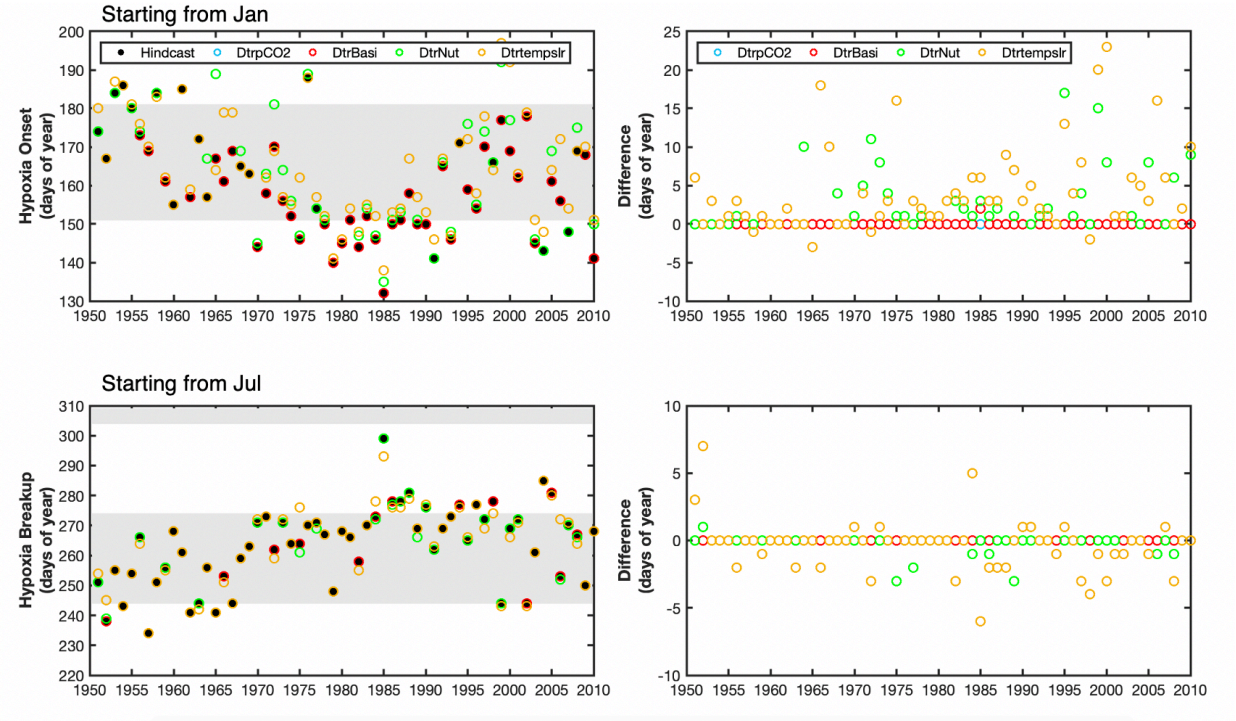

Figure 3.12 Hypoxia onset (a) and breakup (b) timing at CB4.3 from 1951 to 2010 by hindcast run and four scenario runs. The difference of hypoxia onset (c) and breakup (d) timing between $DtrpCO_2$, DtrBasi, DtrNut, Dtrtempslr and Hindcast run correspondingly. The gray and white bars indicate different months.

Table 3.1 Hindcast and scenario run experiments setting

Experiments	Atmospheric pCO2	Riverine TA, pH	Riverine N, P	Temperature & sea-level
Control Experiment (Hindcast run)	1951-2010	1951-2010	1951-2010	1951-2010
Ocean acidification ($DtrpCO_2$ run)	Detrended	1951-2010	1951-2010	1951-2010
River basification (DtrBasi run)	1951-2010	Detrended	1951-2010	1951-2010
Nutrient loading (DtrNut run)	1951-2010	1951-2010	Detrended	1951-2010
Warming & sea-level rise (DtrTempslr run)	1951-2010	1951-2010	1951-2010	Detrended

Chapter 4: Conclusions

In this study, we investigated Chesapeake Bay acidification over a long-term period (1951–2010) using a coupled hydrodynamic-biogeochemical model ROMS-RCA-CC. This long-term retrospective simulation successfully captured seasonal and interannual variations of bottom pH along the central bay from 1951 to 2010, and it also reproduced the expansion of hypoxia with increasing nutrient loading since the 1950s.

The model revealed an overall increasing pH in upper bay and a decreasing pH in lower bay, while the mid-bay pH is relatively more stable over the sixty years. Upper bay pH had a stronger basification signal in spring than in summer. And it increased at a rate of 0.057 to 0.078 units per decade during spring, which could be related to the river basification signal observed in incoming tributaries (Kaushal et al. 2018). Lower bay bottom pH had bigger decreasing rate in summer than spring. In summer, lower bay bottom pH decreased at a rate of -0.033 units per decade and surface water pH decreased at a rate of -0.017 units per decade. Midbay pH showed large fluctuations over the sixty years, and it can be a reflection of the combined impact of local and global pH divers.

Unlike the obvious hypoxia expansion from eutrophication, acidification in Chesapeake Bay did not show a clear expansion over the sixty year. The total acidic volume first decreased from 9.22 km^3 to 7.95 km^3 by 16% from the 1950s to 1970s then increased by 30% to 10.17 km^3 in the 2000s. The overall duration of acidification fluctuated over the six decades and shortened by around one month from the1950s to 2000s with both later onset and earlier termination of about two weeks.

The four senario runs (DtrBais, DtrpCO_2, DtrNut and Dtrtempslr) showed river basification and rising atmospheric pCO_2 were the two largest drivers that control bay-wide acidification. The increasing alkalinized water export from the Susquehanna River not only compensated CO_2-induced acidification but also decrease Chesapeake Bay acidification in terms of total acidic volume and duration. DtrBasi run showed river basification would decrease the summer acidic volume by an average of 44.5% by the 2000s and shorten the acidification duration by one and half month with both later onset and earlier termination of about three weeks. DtrpCO_2 run shows ocean acidification had relatively small influence on upper bay pH as compared to river basification, but it had larger impact decreasing pH in mid and lower bay. The rising atmospheric CO_2 can increase the summer acidic volume by roughly 14.2% and prolong the acidification duration by around two months with earlier initiation of 50 days and later termination of 10 days in end of 2000s.

Both nutrient loading and climate change had nearly no impact on initiation time. But they had different impact on acidification termination. Nutrient loading change can drive a later termination by less than 10 days (with outliers of -35 and -28 in 1975 and 2003). Warming and sea-level rise can bring acidification termination earlier up to 25 days in late summer after 1990. The scenario runs highlighted the importance of riverine basification on Chesapeake Bay acidification and the complex interactions among the local and global drivers on long-term pH trend over the sixty years.

Bibliography

Baumann, H., and E. M. Smith. 2018. Quantifying Metabolically Driven pH and Oxygen Fluctuations in US Nearshore Habitats at Diel to Interannual Time Scales. Estuaries and Coasts 41:1102–1117.

Boesch, D. F., R. B. Brinsfield, and R. E. Magnien. 2001. Chesapeake Bay Eutrophication: Scientific Understanding, Ecosystem Restoration, and Challenges for Agriculture. Journal of Environmental Quality 30:303–320.

Borges, A. V., and N. Gypens. 2010. Carbonate chemistry in the coastal zone responds more strongly to eutrophication than to ocean acidification. Limnology and Oceanography 55:346–353.

Brady, D. C., J. M. Testa, D. M. Di Toro, W. R. Boynton, and W. M. Kemp. 2013. Sediment flux modeling: Calibration and application for coastal systems. Estuarine, Coastal and Shelf Science 117:107–124.

Brodeur, J. R., B. Chen, J. Su, Y. Y. Xu, N. Hussain, M. M. Scaboo, Y. Zhang, J. M. Testa, and W. J. Cai. 2019. Chesapeake bay Inorganic Carbon: Spatial distribution and Seasonal Variability. Frontiers in Marine Science 6:1–17.

Brussaard, C. P. D., G. J. Gast, F. C. Van Duyl, and R. Riegman. 1996. Impact of phytoplankton bloom magnitude on a pelagic microbial food web. Marine Ecology Progress Series 144:211–221.

Cai, W. J., X. Hu, W. J. Huang, M. C. Murrell, J. C. Lehrter, S. E. Lohrenz, W. C. Chou, W. Zhai, J. T. Hollibaugh, Y. Wang, P. Zhao, X. Guo, K. Gundersen, M. Dai, and G. C. Gong. 2011. Acidification of subsurface coastal waters enhanced by eutrophication. Nature Geoscience 4:766–770.

Cai, W. J., W. J. Huang, G. W. Luther, D. Pierrot, M. Li, J. Testa, M. Xue, A. Joesoef, R. Mann, J. Brodeur, Y. Y. Xu, B. Chen, N. Hussain, G. G. Waldbusser, J. Cornwell, and W. Michael Kemp. 2017. Redox reactions and weak buffering capacity lead to acidification in the Chesapeake Bay. Nature Communications 8:1–12.

Carstensen, J., and C. M. Duarte. 2019. Drivers of pH Variability in Coastal Ecosystems. Environmental Science and Technology 53:4020–4029.

Cowan, J. L. W., and W. R. Boynton. 1996. Sediment-water oxygen and nutrient exchanges along the longitudinal axis of Chesapeake Bay: Seasonal patterns, controlling factors and ecological significance. Estuaries 19:562–580.

Dai, M., W. Zhai, W. J. Cai, J. Callahan, B. Huang, S. Shang, T. Huang, X. Li, Z. Lu, W. Chen, and Z. Chen. 2008. Effects of an estuarine plume-associated bloom on the carbonate system in the lower reaches of the Pearl River estuary and the coastal zone of the northern South China Sea. Continental Shelf Research 28:1416–1423.

Ding, H., and A. J. Elmore. 2015. Spatio-temporal patterns in water surface temperature from Landsat time series data in the Chesapeake Bay, U.S.A. Remote Sensing of Environment 168:335–348.

Doney, S. C., V. J. Fabry, R. A. Feely, and J. A. Kleypas. 2009. Ocean acidification: The other CO_2 problem. Annual Review of Marine Science 1:169–192.

Duarte, C. M., I. E. Hendriks, T. S. Moore, Y. S. Olsen, A. Steckbauer, L. Ramajo, J. Carstensen, J. A. Trotter, and M. McCulloch. 2013. Is Ocean Acidification an Open-Ocean Syndrome? Understanding Anthropogenic Impacts on Seawater pH. Estuaries and Coasts 36:221–236.

Egleston, E. S., C. L. Sabine, and F. M. M. Morel. 2010. Revelle revisited: Buffer factors that quantify the response of ocean chemistry to changes in DIC and alkalinity. Global Biogeochemical Cycles 24:1–9.

Ezer, T., and W. B. Corlett. 2012. Is sea level rise accelerating in the Chesapeake Bay? A demonstration of a novel new approach for analyzing sea level data. Geophysical Research Letters 39.

Feely, R. A., S. R. Alin, J. Newton, C. L. Sabine, M. Warner, A. Devol, C. Krembs, and C. Maloy. 2010. The combined effects of ocean acidification, mixing, and respiration on pH and carbonate saturation in an urbanized estuary. Estuarine, Coastal and Shelf Science 88:442–449.

Feely, R. A., C. L. Sabine, J. M. Hernandez-Ayon, D. Ianson, and B. Hales. 2008. Evidence for

upwelling of corrosive “acidified” water onto the continental shelf. Science 320:1490–1492.

Feely, R., T. Klinger, J. Newton, and M. Chadsey. 2012. Scientific Summary of Ocean Acidification in Washington State Marine Waters. Washington State Blue Ribbon Panel on Ocean Acidification. NOAA OAR Special Report:157.

Filippino, K. C., M. R. Mulholland, and P. W. Bernhardt. 2011. Nitrogen uptake and primary productivity rates in the Mid-Atlantic Bight (MAB). Estuarine, Coastal and Shelf Science 91:13–23.

Friedlingstein, P., M. O’Sullivan, M. W. Jones, R. M. Andrew, J. Hauck, A. Olsen, G. P. Peters, W. Peters, J. Pongratz, S. Sitch, C. Le Quéré, J. G. Canadell, P. Ciais, R. B. Jackson, S. Alin, L. E. O. C. Aragão, A. Arneth, V. Arora, N. R. Bates, M. Becker, A. Benoit-Cattin, H. C. Bittig, L. Bopp, S. Bultan, N. Chandra, F. Chevallier, L. P. Chini, W. Evans, L. Florentie, P. M. Forster, T. Gasser, M. Gehlen, D. Gilfillan, T. Gkritzalis, L. Gregor, N. Gruber, I. Harris, K. Hartung, V. Haverd, R. A. Houghton, T. Ilyina, A. K. Jain, E. Joetzjer, K. Kadono, E. Kato, V. Kitidis, J. I. Korsbakken, P. Landschützer, N. Lefèvre, A. Lenton, S. Lienert, Z. Liu, D. Lombardozzi, G. Marland, N. Metzl, D. R. Munro, J. E. M. S. Nabel, S. I. Nakaoka, Y. Niwa, K. O’Brien, T. Ono, P. I. Palmer, D. Pierrot, B. Poulter, L. Resplandy, E. Robertson, C. Rödenbeck, J. Schwinger, R. Séférian, I. Skjelvan, A. J. P. Smith, A. J. Sutton, T. Tanhua, P. P. Tans, H. Tian, B. Tilbrook, G. Van Der Werf, N. Vuichard, A. P. Walker, R. Wanninkhof, A. J. Watson, D. Willis, A. J. Wiltshire, W. Yuan, X. Yue, and S. Zaehle. 2020. Global Carbon Budget 2020. Earth System Science Data 12:3269–3340.

Gattuso, J.-P., M. Frankignoulle, and R. Wollast. 1998. CARBON AND CARBONATE METABOLISM IN COASTAL AQUATIC ECOSYSTEMS.

Gilbert, R. O. 1987. Statistical methods for environmental pollution monitoring. John Wiley & Sons.

Gomez, F. A., R. Wanninkhof, L. Barbero, and S. K. Lee. 2021, December 28. Increasing River Alkalinity Slows Ocean Acidification in the Northern Gulf of Mexico. John Wiley & Sons, Ltd.

Hagens, M., C. P. Slomp, F. J. R. Meysman, D. Seitaj, J. Harlay, A. V. Borges, and J. J. Middelburg. 2015. Biogeochemical processes and buffering capacity concurrently affect acidification in a seasonally hypoxic coastal marine basin. Biogeosciences 12:1561–1583.

Hagy, J. D., W. R. Boynton, C. W. Keefe, and K. V. Wood. 2004. Hypoxia in Chesapeake Bay, 1950-2001: Long-term change in relation to nutrient loading and river flow. Estuaries 27:634–658.

Harris, K. E., M. D. DeGrandpre, and B. Hales. 2013. Aragonite saturation state dynamics in a coastal upwelling zone. Geophysical Research Letters 40:2720–2725.

Hastie, T. J., and R. J. Tibshirani. 2017. Generalized additive models. Routledge.

Hauri, C., N. Gruber, M. Vogt, S. C. Doney, R. A. Feely, Z. Lachkar, A. Leinweber, A. M. P. McDonnell, and M. Munnich. 2013. Spatiotemporal variability and long-term trends of ocean acidification in the California Current System. Biogeosciences 10:193–216.

Hofmann, G. E., J. E. Smith, K. S. Johnson, U. Send, L. A. Levin, F. Micheli, A. Paytan, N. N. Price, B. Peterson, Y. Takeshita, P. G. Matson, E. de Crook, K. J. Kroeker, M. C. Gambi, E. B. Rivest, C. A. Frieder, P. C. Yu, and T. R. Martz. 2011. High-frequency dynamics of ocean pH: A multi-ecosystem comparison. PLoS ONE 6.

Hu, X., and W. J. Cai. 2013. Estuarine acidification and minimum buffer zone - A conceptual study. Geophysical Research Letters 40:5176–5181.

Huang, W. J., W. J. Cai, X. Xie, and M. Li. 2019. Wind-driven lateral variations of partial pressure of carbon dioxide in a large estuary. Journal of Marine Systems 195:67–73.

James, G., D. Witten, T. Hastie, and R. Tibshirani. 2013. An introduction to statistical learning. Springer.

Johnson, Z. I., B. J. Wheeler, S. K. Blinebry, C. M. Carlson, C. S. Ward, and D. E. Hunt. 2013. Dramatic variability of the carbonate system at a temperate coastal ocean site (Beaufort, North Carolina, USA) is regulated by physical and biogeochemical processes on multiple timescales. PLoS ONE 8:1–8.

Kaushal, S. S., G. E. Likens, M. L. Pace, R. M. Utz, S. Haq, J. Gorman, and M. Grese. 2018.

Freshwater salinization syndrome on a continental scale. Proceedings of the National Academy of Sciences of the United States of America 115:E574–E583.

Kaushal, S. S., G. E. Likens, R. M. Utz, M. L. Pace, M. Grese, and M. Yepsen. 2013. Increased river alkalinization in the eastern U.S. Environmental Science and Technology 47:10302–10311.

Kemp, W. M., W. R. Boynton, J. E. Adolf, D. F. Boesch, W. C. Boicourt, G. Brush, J. C. Cornwell, T. R. Fisher, P. M. Glibert, J. D. Hagy, L. W. Harding, E. D. Houde, D. G. Kimmel, W. D. Miller, R. I. E. Newell, M. R. Roman, E. M. Smith, and J. C. Stevenson. 2005a. Eutrophication of Chesapeake Bay: Historical trends and ecological interactions. Marine Ecology Progress Series 303:1–29.

Kemp, W. M., W. R. Boynton, J. E. Adolf, D. F. Boesch, W. C. Boicourt, G. Brush, J. C. Cornwell, T. R. Fisher, P. M. Glibert, J. D. Hagy, L. W. Harding, E. D. Houde, D. G. Kimmel, W. D. Miller, R. I. E. Newell, M. R. Roman, E. M. Smith, and J. C. Stevenson. 2005b, November 21. Eutrophication of Chesapeake Bay: Historical trends and ecological interactions. Inter-Research.

Kendall, M. G. 1948. Rank correlation methods.

Laurent, A., K. Fennel, W. J. Cai, W. J. Huang, L. Barbero, and R. Wanninkhof. 2017. Eutrophication-induced acidification of coastal waters in the northern Gulf of Mexico: Insights into origin and processes from a coupled physical-biogeochemical model. Geophysical Research Letters 44:946–956.

Lewis, E. ., and D. W. . Wallace. 1998. CO2SYS-Program developed for CO_2 system calculations.

Li, M., L. Zhong, and W. C. Boicourt. 2005. Simulations of Chesapeake Bay estuary: Sensitivity to turbulence mixing parameterizations and comparison with observations. Journal of Geophysical Research: Oceans 110:1–22.

Logan, C. A. 2010. A review of Ocean acidification and America's Response. BioScience 60:819–828.

Mann, H. B. 1945. Nonparametric Tests Against Trend. Econometrica 13:245.

Müller, J. D., B. Schneider, and G. Rehder. 2016. Long-term alkalinity trends in the Baltic Sea and their implications for CO_2-induced acidification. Limnology and Oceanography 61:1984–2002.

Orr, J. C., V. J. Fabry, O. Aumont, L. Bopp, S. C. Doney, R. A. Feely, A. Gnanadesikan, N. Gruber, A. Ishida, F. Joos, R. M. Key, K. Lindsay, E. Maier-Reimer, R. Matear, P. Monfray, A. Mouchet, R. G. Najjar, G. K. Plattner, K. B. Rodgers, C. L. Sabine, J. L. Sarmiento, R. Schlitzer, R. D. Slater, I. J. Totterdell, M. F. Weirig, Y. Yamanaka, and A. Yool. 2005. Anthropogenic ocean acidification over the twenty-first century and its impact on calcifying organisms. Nature 437:681–686.

Osburn, C. L., J. C. Rudolph, H. W. Paerl, A. G. Hounshell, and B. R. Van Dam. 2019. Lingering Carbon Cycle Effects of Hurricane Matthew in North Carolina's Coastal Waters. Geophysical Research Letters 46:2654–2661.

Paerl, H. W., J. R. Crosswell, B. Van Dam, N. S. Hall, K. L. Rossignol, C. L. Osburn, A. G. Hounshell, R. S. Sloup, and L. W. Harding. 2018. Two decades of tropical cyclone impacts on North Carolina's estuarine carbon, nutrient and phytoplankton dynamics: implications for biogeochemical cycling and water quality in a stormier world. Biogeochemistry 141:307–332.

Provoost, P., S. Van Heuven, K. Soetaert, R. W. P. M. Laane, and J. J. Middelburg. 2010. Seasonal and long-term changes in pH in the Dutch coastal zone. Biogeosciences 7:3869–3878.

Raymond, P. A., and J. J. Cole. 2003. Increase in the export of alkalinity from North America's largest river. Science 301:88–91.

Raymond, P. A., and N. H. Oh. 2009. Long term changes of chemical weathering products in rivers heavily impacted from acid mine drainage: Insights on the impact of coal mining on regional and global carbon and sulfur budgets. Earth and Planetary Science Letters 284:50–56.

Raymond, P. A., N. H. Oh, R. E. Turner, and W. Broussard. 2008. Anthropogenically enhanced fluxes of water and carbon from the Mississippi River. Nature 451:449–452.

Rice, K. C., and J. D. Jastram. 2015. Rising air and stream-water temperatures in Chesapeake Bay region, USA. Climatic Change 128:127–138.

Sabine, C. L., R. A. Feely, N. Gruber, R. M. Key, K. Lee, J. L. Bullister, R. Wanninkhof, C. S. Wong, D. W. R. Wallace, B. Tilbrook, F. J. Millero, T. H. Peng, A. Kozyr, T. Ono, and A. F. Rios. 2004. The oceanic sink for anthropogenic CO_2. Science 305:367–371.

Salisbury, J., M. Green, C. Hunt, and J. Campbell. 2008. Coastal Acidification by Rivers:A Threat to Shellfish? Eos, Transactions American Geophysical Union 89:513–513.

Schulz, K. G., S. Hartley, and B. Eyre. 2019. Upwelling Amplifies Ocean Acidification on the East Australian Shelf: Implications for Marine Ecosystems. Frontiers in Marine Science 6:1–8.

Semiletov, I., I. Pipko, Ö. Gustafsson, L. G. Anderson, V. Sergienko, S. Pugach, O. Dudarev, A. Charkin, A. Gukov, L. Bröder, A. Andersson, E. Spivak, and N. Shakhova. 2016. Erratum: Acidification of East Siberian Arctic Shelf waters through addition of freshwater and terrestrial carbon (Nature Geoscience (2016) 9 (361-365)). Nature Geoscience 9:368.

Sen, P. K. 1968. Estimates of the regression coefficient based on Kendall's tau. Journal of the American statistical association 63:1379–1389.

Shen, C., J. M. Testa, M. Li, and W. Cai. 2020. Understanding anthropogenic impacts on pH and aragonite saturation in Chesapeake Bay: insights from a 30-year model study. Journal of Geophysical Research: Biogeosciences.

Shen, C., J. M. Testa, M. Li, W. J. Cai, G. G. Waldbusser, W. Ni, W. M. Kemp, J. Cornwell, B. Chen, J. Brodeur, and J. Su. 2019a. Controls on Carbonate System Dynamics in a Coastal Plain Estuary: A Modeling Study. Journal of Geophysical Research: Biogeosciences 124:61–78.

Shen, C., J. M. Testa, M. Li, W. J. Cai, G. G. Waldbusser, W. Ni, W. M. Kemp, J. Cornwell, B. Chen, J. Brodeur, and J. Su. 2019b. Controls on Carbonate System Dynamics in a Coastal Plain Estuary: A Modeling Study. Journal of Geophysical Research: Biogeosciences 124:61–78.

Shen, C., J. M. Testa, W. Ni, W. J. Cai, M. Li, and W. M. Kemp. 2019c. Ecosystem Metabolism

and Carbon Balance in Chesapeake Bay: A 30-Year Analysis Using a Coupled Hydrodynamic-Biogeochemical Model. Journal of Geophysical Research: Oceans 124:6141–6153.

Soetaert, K., K. Soetaert, A. F. Hofmann, A. F. Hofmann, J. J. Middelburg, J. J. Middelburg, F. J. R. Meysman, F. J. R. Meysman, J. Greenwood, and J. Greenwood. 2007. The effect of biogeochemical processes on pH. Marine Chemistry 105:30–51.

Sprague, L. a., M. J. Langland, S. E. Yochum, R. E. Edwards, J. D. Blomquist, S. W. Phillips, G. W. Shenk, and S. D. Preston. 2000. Factors affecting nutrient trends in major rivers of the Chesapeake Bay Watershed:109.

St-Laurent, P., M. A. M. Friedrichs, R. G. Najjar, E. H. Shadwick, H. Tian, and Y. Yao. 2020. Relative impacts of global changes and regional watershed changes on the inorganic carbon balance of the Chesapeake Bay. Biogeosciences 17:3779–3796.

Sunda, W. G., and W. J. Cai. 2012. Eutrophication induced CO_2-Acidification of subsurface coastal waters: Interactive effects of temperature, salinity, and atmospheric PCO_2. Environmental Science and Technology 46:10651–10659.

Testa, J. M., D. C. Brady, D. M. Di Toro, W. R. Boynton, J. C. Cornwell, and W. M. Kemp. 2013. Sediment flux modeling: Simulating nitrogen, phosphorus, and silica cycles. Estuarine, Coastal and Shelf Science 131:245–263.

Theil, H. 1950. A rank-invariant method of linear and polynomial regression analysis. Indagationes mathematicae 12:173.

Waldbusser, G. G., E. P. Voigt, H. Bergschneider, M. A. Green, and R. I. E. Newell. 2011. Biocalcification in the Eastern Oyster (Crassostrea virginica) in Relation to Long-term Trends in Chesapeake Bay pH. Estuaries and Coasts 34:221–231.

Wallace, R. B., H. Baumann, J. S. Grear, R. C. Aller, and C. J. Gobler. 2014. Coastal ocean acidification: The other eutrophication problem. Estuarine, Coastal and Shelf Science 148:1–13.

Weiss, R. 1974. Carbon dioxide in water and seawater: the solubility of a non-ideal gas. Marine chemistry 2:203–215.

Wilcox, R. R. 2001. Fundamentals of modern statistical methods: Substantially improving power and accuracy. Springer.

Wood, S. N. 2006. Generalized additive models: an introduction with R. chapman and hall/CRC.

Xu, Y. Y., W. J. Cai, R. Wanninkhof, J. Salisbury, J. Reimer, and B. Chen. 2020. Long-Term Changes of Carbonate Chemistry Variables Along the North American East Coast. Journal of Geophysical Research: Oceans 125.

Zhang, Q., D. C. Brady, W. R. Boynton, and W. P. Ball. 2015. Long-Term Trends of Nutrients and Sediment from the Nontidal Chesapeake Watershed: An Assessment of Progress by River and Season. Journal of the American Water Resources Association 51:1534–1555.

Zhong, L., and M. Li. 2006. Tidal energy fluxes and dissipation in the Chesapeake Bay. Continental Shelf Research 26:752–770.